



**Politecnico
di Torino**

POLITECNICO DI TORINO

Collegio di Ingegneria Informatica, del Cinema e Meccatronica

MASTER'S DEGREE IN MECHATRONIC ENGINEERING

Low voltage inverter for mechatronic actuation systems

Author:

Erasmus D'Alessandro

Supervisor:

Prof. Andrea Tonoli

Co-supervisors:

Prof. Renato Galluzzi

Prof. Luis Miguel Ibarra
Moyers

ACADEMIC YEAR 2022/2023

ABSTRACT:

The scope of this thesis work is to implement a complete design of a low voltage inverter in general for any type of mechatronic system, although in this case the application is about three-phase motor of an e-bike.

Structure and main arguments:

The work is structured in three phases: a brief introduction with some research about the existing circuits and the required electronics, the electronic design and some tests and simulations, the PCB design and final results.

- In the first part there are some descriptions about the typical problems related to the electronic devices used in the inverter design (in particular, the gate drivers have a lot of details to be careful) like current and voltage values or switching frequencies and so on.
- For the electronic design, after a comparison of different gate drivers and power MOSFETs through datasheet of these components, I have verified with a Simulink model some important parameters, like current limits and delays, of the total system or specific components. I have checked also other device performances to be sure that the selected components are the best for this application. At the end of this part, I have obtained the final model composed by the micro controller, the inverter and the motor load.
- In the final part I have built the total PCB of the inverter using the main devices previously chosen. All the steps to draw the schematic with all the connection between the components have been described and all the design choices have been justified. At the end, starting from the schematic the printed circuit has been obtained, selecting the appropriate footprints for each component, placing them in a correct way, respecting all design rules for drawing all the tracks. The design choices have been done also considering the overheat problems, for example the tracks width, the temperature parameters of each device and so on. But to be sure that all the components don't get too hot, and in general the entire PCB has a proper thermal performance, it would be necessary to carry out a thermal validation in such a way as to be able to actually produce the real final printed circuit.

Contents:

1. Introduction	6
1.1. State of the art: mechatronic solutions.....	6
1.2. Automotive systems, 48 V actuators, e-bike applications	9
1.3. Problems (high f_{sw} , high currents, MOSFETs).....	10
1.4. General structure of the system, overview on the required electronics ...	11
1.5. Thesis structure	13
2. Design	14
2.1. Controlled Load	14
2.2. Component selection.....	16
2.3. Simulink model (gate driver - power MOSFET - battery load)	23
2.4. First simulation using the driver and the MOSFET initially chosen	25
2.5. Second simulation using the new driver and MOSFET	29
2.6. Graphic representation and tables with delays measurement.....	31
3. Results	34
3.1. The final PCB, with design comments	34
3.2. Bill of materials	49
4. Conclusions	53
5. References	54

LIST OF FIGURES:

Figure 1 - High voltage power devices mapping (Power vs Frequency) [5].	7
Figure 2 - General structure of the system, from DRV832x Smart Gate Driver datasheet, Texas Instruments [6].	11
Figure 3 - Simple schematic of the main inverter subsystems, and their related functions [7].	12
Figure 4 - Radial view (on the left) and axial view (on the right).	14
Figure 5 – Phase RMS current map of the motor in torque – angular speed area.	15
Figure 6 - Maximum safe operating area.	16
Figure 7 - Shoot through condition, inductive spiking and coupling from switching on MOSFET.	19
Figure 8 - Gate resistors, sink and source resistors when gate current is fixed.	20
Figure 9 - Simulink scheme of gate driver - power MOSFET system.	23
Figure 10 - Simulink scope, first simulation.	25
Figure 11 - First simulation (zoom, driver propagation delay).	26
Figure 12 - First simulation (zoom, rise and fall time).	26
Figure 13 - Simulink scheme, adding two 5 Ohm resistors and one diode between the driver and the MOSFET.	27
Figure 14 - Second simulation, within the resistances and the diode.	27
Figure 15 - Second simulation, with 10 Ohm resistors.	28
Figure 16 - Third simulation, CSD19536KTT MOSFET and 5 Ohm resistors.	29
Figure 17 - Third simulation, CSD19536KTT MOSFET and 10 Ohm resistors.	30
Figure 18 - Fourth simulation, UCC27282-Q1 + CSD88599Q5DC + 5 Ohm resistors.	31
Figure 19 - Fourth simulation, UCC27282-Q1 + CSD19536KTT + 5 Ohm resistors.	31
Figure 20 - Overall system with main connections between PCB and external components.	34
Figure 21 - The general circuit with all the symbols and their connections, screen taken from schematic editor in KiCad.	35
Figure 22 - Zoom on the connection between the LaunchPad connectors and the gate drivers.	36
Figure 23 - Zoom on the connection between the gate drivers and the power MOSFETs.	37
Figure 24 - Zoom on the phase voltage/current sense circuit.	38
Figure 25 - Zoom on the Over Current Protection (OCP) circuit.	38
Figure 26 - Zoom on the DC/DC converter.	40
Figure 27 - DC-DC converter scheme from TPS54060 datasheet.	40
Figure 28 - f_{sw} vs R_T/CLK resistance in low frequency range, from TPS54060 datasheet.	41
Figure 29 - Electrical circuit of the internal step-up voltage regulator (LMR62421) in the Launchpad.	42
Figure 30 - Board stackup – Physical stackup from PCB editor.	44
Figure 31 - Printed Circuit Board of the total inverter with all the footprints and the tracks, screen taken from PCB editor in KiCad.	45
Figure 32 - zoom on the motor power tracks.	46
Figure 33 - zoom on the supply power tracks.	47

LIST OF TABLES:

Table 1 - Base speed point, from motor datasheet (6.0 A/mm ² current density).	14
Table 2 - Base speed point, from motor datasheet (20.0 A/mm ² maximum current density)	15
Table 3 - Maximum speed point, from motor datasheet	15
Table 4 - Absolute maximum ratings from the CSD18536KCS datasheet [16].	16
Table 5 - Absolute maximum ratings of the CSD19535KCS MOSFET, from the datasheet [15].	17
Table 6 - Main dynamic characteristics.	17
Table 7 - Absolute maximum ratings of the CSD19536KTT power MOSFET [14].	17
Table 8 - Main dynamic characteristics.	18
Table 9 - Main parameters from CSD88599Q5DC datasheet [13].	24
Table 10 - Gate Driver block parameters.	24
Table 11 - Main MOSFET block parameters from CSD19536KTT datasheet.	29
Table 12 - Main driver block parameters.	30
Table 13 - Time delays using the DRV8323 smart gate driver.	32
Table 14 - Time delays using the UCC27282-Q1 gate driver.	32
Table 15 - Dynamic characteristics table from the NOR port datasheet.	39
Table 16 - Heat sink parameters from the datasheet.	48
Table 17 - Inverter PCB bill of materials	49

1. Introduction

1.1. State of the art: mechatronic solutions

Today, in most electronic devices and in general in many applications, it is often required a lot of power. At the same time these applications are also reducing in overall size. One way to achieve both high power and low size is to improve the efficiency and distribute the power loss optimally.

Most of these applications employ power MOSFETs and they are being switched at higher and higher frequencies. To operate power MOSFETs at high switching frequencies and to reduce associated switching losses, a powerful gate driver is employed between the PWM output of the controller and the gates of the power semiconductor devices, such as power MOSFETs, IGBTs, SiC FETs and GaN FETs. Many of these applications require proper undervoltage-lockout (UVLO) protection so that power semiconductor devices are turned ON and OFF optimally.

Also, gate drivers are indispensable when it is impossible for the PWM controller to directly drive the gates of the switching devices. With the advent of digital power, this situation is often encountered because the PWM signal from the digital controller is often a 3.3-V logic signal which cannot effectively turn on a power switch. A level-shift circuit is needed to boost the 3.3-V signal to the gate-drive voltage (such as 12 V or 5 V) in order to fully turn-on the power device, minimize conduction losses, and minimize the switching losses.

Traditional buffer drive circuits based on NPN/PNP bipolar transistors in totem-pole arrangement prove inadequate with digital power because they lack level-shifting capability and undervoltage-lockout protection. Gate drivers effectively combine both the level-shifting and buffer-drive functions.

Gate drivers also solve other problems such as minimizing the effect of high-frequency switching noise (by placing the high-current driver device physically close to the power switch), driving gate-drive transformers and controlling floating power device gates. This helps reduce power dissipation and thermal stress in controllers by moving gate charge power losses from the controller IC to the gate driver.

A lot of applications which use gate drivers and power switches are in the e-mobility area.

In fact, thinking about hybrid and electric vehicles, they need power converters. Precisely there are three types of power converters located in a vehicle: AC-DC converters (rectifiers), DC-DC converters and DC-AC converters (inverters).

The inverter is the most important power converter which converts a DC input voltage to the required magnitude and frequency of AC output voltage.

For example, in BEV (battery electric vehicle) the stored energy must be converted from DC to AC to drive AC motor. This DC-AC converters are called traction inverters and transfer power of tens kW up to 50 kW. In these inverter topologies the IGBTs (insulated gate bipolar transistors) are used and the typical voltage level are 600-1200V. The three-phase full bridge inverter uses six semiconductor power devices for driving electrical motors.

For each phase there is a lower and higher side IGBT switch and the typical switching frequencies are between 5 and 20 kHz.

Now, the most advanced power converter used in electrified vehicles and industry are the two-level inverters [1]. Also the power devices used are not the optimal ones because the IGBTs have high losses so it is better to use power MOSFETs at a lower voltage level.

As said before, there also other new power semiconductor devices like SiC and GaN FETs [2], they are faster switching speed and higher power density, in particular GaN is better than SiC device.

GaN-FET has smaller on-resistance and junction capacitance and it has a turn-on and turn-off speed of several nanoseconds. But during the switching process an overshoot oscillation can occurs and extra losses and voltage stress are added to the switch in the transient pulsed loop.

In general, MOSFETs are used with designs involving relatively lower voltage and power requirements but Silicon carbide (SiC) MOSFETs have a critical breakdown strength that is 10x of silicon, they can operate at much higher temperatures, provide higher current density, experience reduced switching losses and support higher switching frequencies. This also means that silicon carbide MOSFETs are more similar to silicon IGBTs, and in many designs, can replace silicon IGBTs while offering additional benefits to the total design [3].

Silicon carbide MOSFETs outperform their silicon counterparts in other ways, including the ability to handle higher voltage and power requirements while still saving space. The use of silicon carbide makes these MOSFETs extremely rugged and durable.

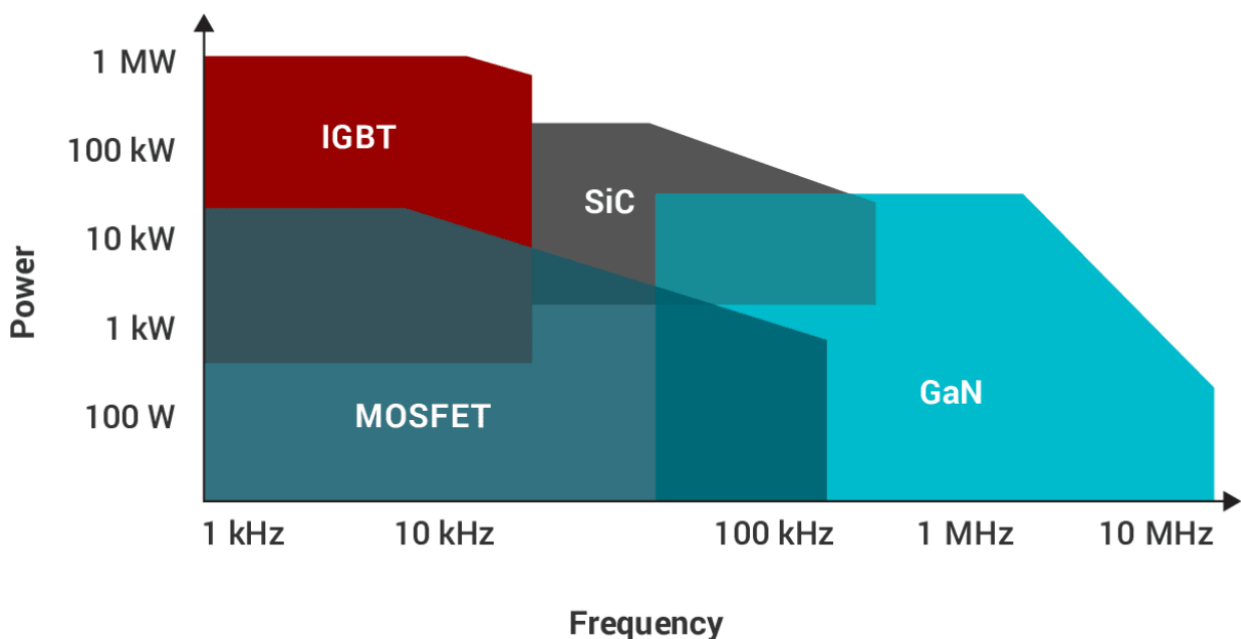


Figure 1 - High voltage power devices mapping (Power vs Frequency) [5].

As the figure 1 shows, each device has different power and frequency range.

The main differences are between the power MOSFET and the IGBT. The first device operates up to tens of kW but at hundreds of kHz of frequency, instead the IGBT is able to handle high powers (up to 1 MW) but it has low limits for the frequency (in the typical applications these devices don't go beyond 20 kHz).

If high powers and frequencies are needed, it is necessary to change device and use the new power switches like GaN and SiC FETs. The SiC almost reaches the same powers of the IGBT devices but it can work at frequencies over 100 kHz. The GaN technology uses very high frequencies up to 10 MHz, but it doesn't support very high operating powers (slightly higher than the MOSFET limits) [5].

1.2. Automotive systems, 48 V actuators, e-bike applications

The main applications where these devices (gate drivers and power devices, mentioned in the previous section) are used are the automotive systems, for example the brushless-DC (BLDC) motor modules or the permanent magnet synchronous motor (PMSM). In general, these types of motor are supplied by 48 V, in other case 24 and 36 V. There are many other types of applications like fans, pumps, servo drives, e-bikes, e-scooters, e-mobility, cordless garden, power tools, lawnmowers, cordless vacuum cleaners. Also, in robotics environment like drones, industrial and logistics robots.

Still regarding automotive DC/DC converters, electric power steering, on-board charger (OBC), integrated belt starter generator (iBSG), automotive HVAC compressor modules.

All the applications mentioned using power MOSFETs as high frequency switching devices and gate driver between microcontroller and power device.

Today, there is an increasing voltage values for the electric vehicle, where the manufacturers increase the battery pack voltage. A high-voltage battery pack reduces the current required to transfer the same power at a lower voltage and thus offers benefits such as lower run-time ohmic losses, very low DC fast charging duration, and reduction in the overall weight of the powertrain conductors [4].

The same considerations can be done in e-bike applications where higher voltages can be used to substitute the low voltage systems. The benefits are all those listed above and there are all the reasons to change the battery voltage and if it is necessary all the system, included electric motor and power inverter. But a battery pack of 48V is greater than the 24V or 36V ones because to obtain a higher voltage more piles in series are needed and this implies a bulkier battery which is not always the best solution in e-bike applications.

For this project the load of the entire system is an electric motor used mostly in the e-bikes, but the inverter designed could be also used for other applications paying attention to the proper sizing in relation to the electrical parameters or the specifications required.

1.3. Problems (high f_{sw} , high currents, MOSFETs)

The most frequent problems designing low power inverters are the current limits and the switching frequency.

When dealing with motor applications the system designers must pay attention to solve some challenges which are fundamentals during the inverter stage design. These challenges include slew rate control setting this feature to optimize switching performance, managing MOSFET and all the protections needed, and driver timing performance improvement for motor control.

The main parameters to be calculated and analysed are the MOSFET V_{DS} slew rates and the gate drive currents. There are two types of gate drive current: the peak gate drive current and the average gate drive current.

The peak gate drive current is the maximum current that the gate driver can source or sink to the power MOSFET gate during the turn on and turn off events, and this parameter is important because it tells us how fast the power device can slew.

Instead, the average gate drive current is the average current needed by the driver to switch the power MOSFET constantly.

In the “Driver problems” section some formulas and approximated calculations are done to give a general idea how these parameters must be set and how they change the overall system behaviour.

But the most crucial actions to consider are the adjustment and tuning of the MOSFET slew rate because it directly related to the switching power dissipation, radiated emissions, inductive voltage spikes and dV/dt parasitic turn on. Slower slew rates improve all these performances but increase power dissipation, so the task of the motor system designer is to find the best trade off, which satisfies all these stuffs.

1.4. General structure of the system, overview on the required electronics

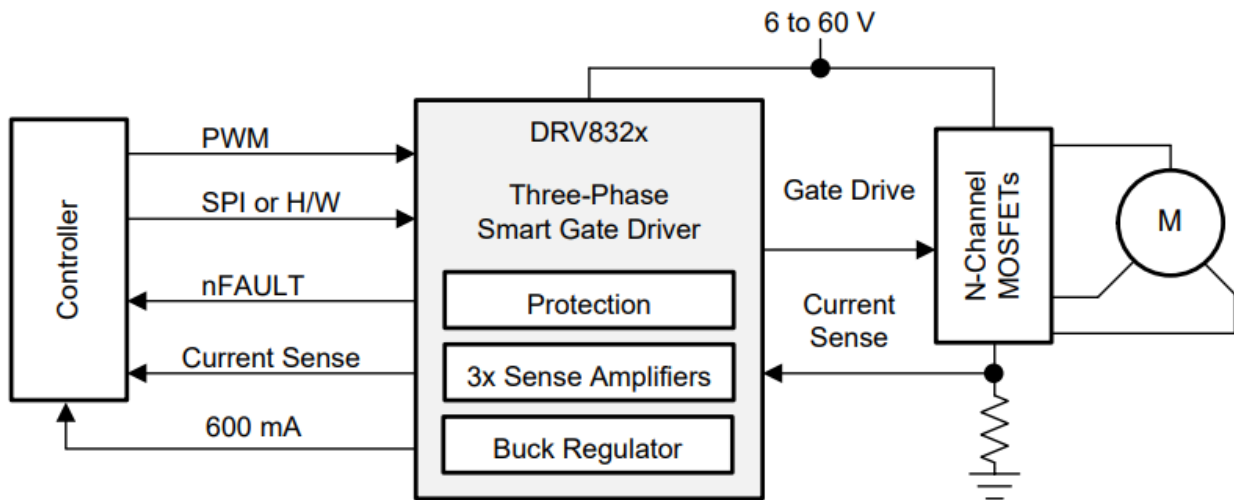


Figure 2 - General structure of the system, from DRV832x Smart Gate Driver datasheet, Texas Instruments [6].

The overall system includes four main parts.

Starting from the left there is the controller, which is the “brain” of the system and it manages all the control signals (PWM) to send to the driver or to be received.

The gate driver connects the control to the power part, so it has three high accuracy trimmed and temperature compensated half bridge drivers, each capable of driving a high-side and low-side N-type MOSFET. The buck regulator is used to obtain the required low voltage, three sense amplifiers to control the current values from the motor and a protection circuit to avoid internal damages.

The power devices that act as switches of the three motor phases. This part is composed of six N-Channel MOSFETs, two (high and low side) for each phase of the motor.

The load is a three-phase motor, all the specifications are described in the dedicated section.

Regarding the required electronics, the total system can be divided into three main subsystems: the control system, the inverter and the load.

The control system is obviously the microcontroller. In this project the microcontroller used is the C2000 LAUNCHXL-F28379D Launchpad, which is a complete low-cost development board for the Texas Instruments Delfino F2837xD devices. The LAUNCHXL-F28379D [11] kit features all the hardware and software necessary to develop applications based on the F2837xD microcontrollers. The Launchpad provides the system with all the control logic. Precisely, thanks to the PWM signals

the microcontroller is able to control the switching operation of the power devices connected to the motor.

Then the central part is dedicated to the inverter design, so it needs of three gate drivers, each able to drive two power devices (one high side MOSFET and one low side) that are the switches that control the three phases of the motor. The inverter has three main tasks: the first is to deliver current to the motor, the second is to translate the digital logic PWM input signals to signals at a higher analog voltage level (in this case 48V), the third is to control the signals at the power device gates adding specialized protection circuit.

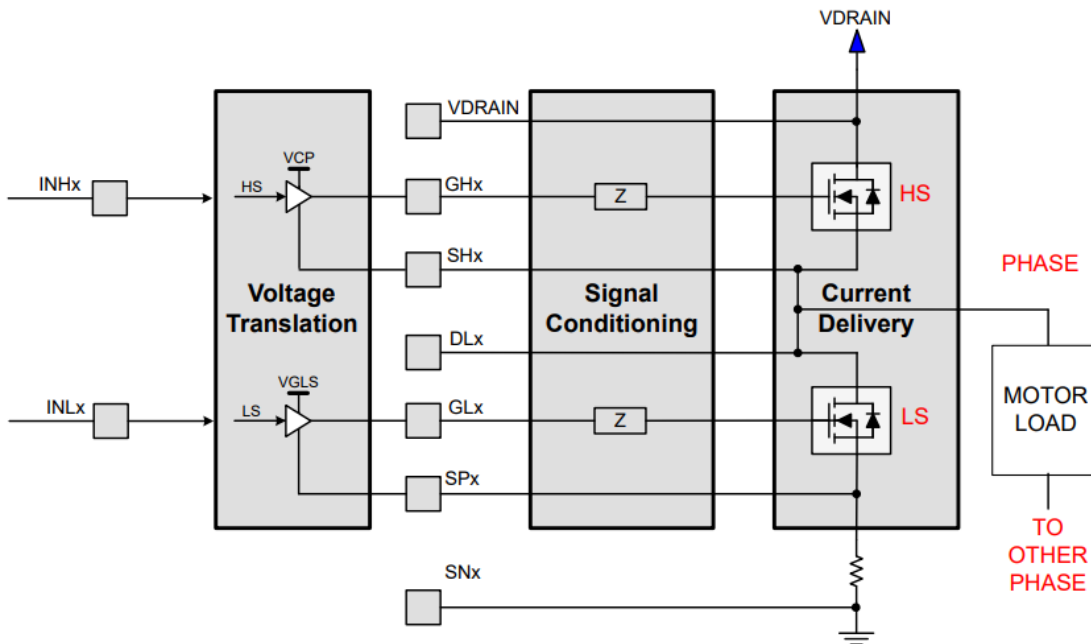


Figure 3 - Simple schematic of the main inverter subsystems, and their related functions [7].

The final part of the system is the load that must be connected to the inverter to be controlled. In this project the load is an electric motor, mainly used in the e-bikes.

In the “Design” section all the electric motor specifications have been described.

1.5. Thesis structure

The thesis is articulated in four main chapters:

- **Chapter 1:** The first chapter is the introduction of the project thesis. Th state of the art of the actual mechatronic solutions and the typical applications used in these and next years. Some power devices comparison and their use in the motor control systems. The main parameters which must be considered when working with the power electronics devices. At the end, the general structure of the entire system is shown and the required components used to design it.
- **Chapter 2:** The second chapter describes all the design steps of the project. In particular, starting from some requirements, where the most important is the motor datasheet, it is explained how all the components have been chosen. Some simulations have been executed and the final results for each device have been reported in graphs and in resuming tables where comparisons between different components (drivers and MOSFETs) can be analysed to choose the best devices to use in the inverter design.
- **Chapter 3:** In the third chapter, the part related to the final results, the total electronic system has been physically built in a PCB. So, in this part, all the PCB design choices with all the considerations are reported. This part also includes the bill of materials and the estimated cost of the overall system.
- **Chapter 4:** The final chapter is inherent to the final considerations made for the model built and a final comment about the work performed.

2. Design

2.1. Controlled Load

The total circuit to be designed is composed by three main parts. The first is the microcontroller that in this case is the launchpad. The central part is the inverter composed by gate drivers and power MOSFETs. The third and final part is the motor that is the load of the system.

Starting right from the analysis of some important characteristics of the motor, in the datasheet, the choice of components can be made in the best way.

The motor used for this application is a 3-phase synchronous machine, permanent magnet, inner rotor.

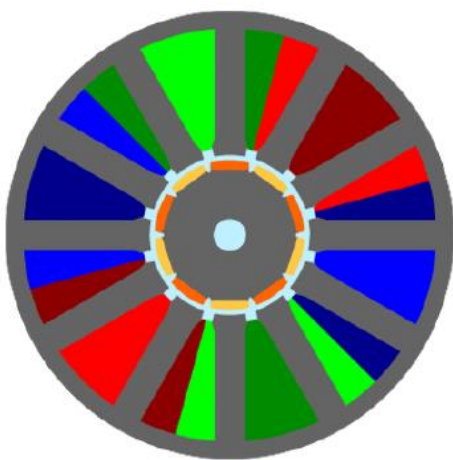


Fig. 1 Radial view

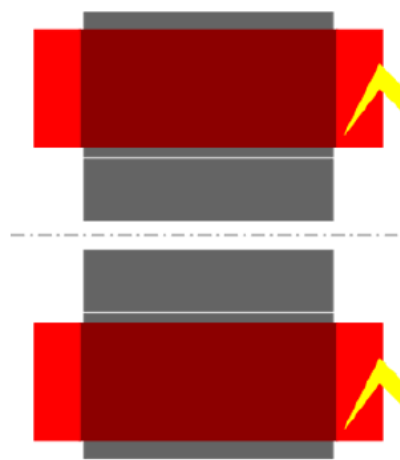


Fig. 2 Axial view

Figure 4 - Radial view (on the left) and axial view (on the right).

From machine performance table in the datasheet, in case of base speed point, the main parameters are (also reported in the bottom table):

torque = 2.6 Nm, speed = 4364.807 rpm, electrical frequency = 363.734 Hz, RMS current = 25.918 A, line-line RMS voltage = 33.94 V (so the nominal voltage of the motor is 48 V).

The normal situation of the motor is at current density of 6.0 A/mm², so the parameters are measured in this condition.

Table 1 - Base speed point, from motor datasheet (6.0 A/mm² current density).

Name	Value	Name	Value
Mechanical torque	2.6 Nm	Speed	4364.807 rpm
Mechanical power	1188.216 W	Machine electrical power	1268.194 W
Line current (RMS)	25.918 A	Phase current (RMS)	25.918 A
Line-line voltage (RMS)	33.94 V	Phase voltage (RMS)	19.595 V
Current density (RMS)	6.0 A/mm ²	Electrical frequency	363.734 Hz

Instead at max current density of 20 A/mm² and with torque = 6.767 Nm, speed = 3022.248 rpm and frequency = 251.854 Hz, the current is equal to 86.394 A (very high respect to the first case!).

Table 2 - Base speed point, from motor datasheet (20.0 A/mm² maximum current density)

Name	Value	Name	Value
Mechanical torque	6.767 Nm	Speed	3022.248 rpm
Mechanical power	2141.609 W	Machine electrical power	2585.136 W
Line current (RMS)	86.394 A	Phase current (RMS)	86.394 A
Line-line voltage (RMS)	33.94 V	Phase voltage (RMS)	19.595 V
Current density (RMS)	20.0 A/mm ²	Electrical frequency	251.854 Hz

Another relevant case to analyse is when the motor is at his maximum speed point, at 20000 rpm. In this case the RMS current is 37.924 A, but the main parameter to be considered is the electrical frequency that is 1666.667 Hz.

Table 3 - Maximum speed point, from motor datasheet

Name	Value	Name	Value
Mechanical torque	0.8656 Nm	Speed	20000.0 rpm
Mechanical power	1812.859 W	Machine electrical power	2164.755 W
Line current (RMS)	37.924 A	Phase current (RMS)	37.924 A
Line-line voltage (RMS)	33.94 V	Phase voltage (RMS)	19.595 V
Current density (RMS)	20.0 A/mm ²	Electrical frequency	1666.667 Hz

In order to set the PWM signal frequency for the control, it is usual to choose a frequency at least ten time bigger than this value, for example 16 kHz or better 20 kHz.

All these informations and parameters analyzed before can also be reported using the flux maps. The following flux map shows how the torque and current vary in function of the motor speed, the two main points (base and maximum speed) are highlighted.

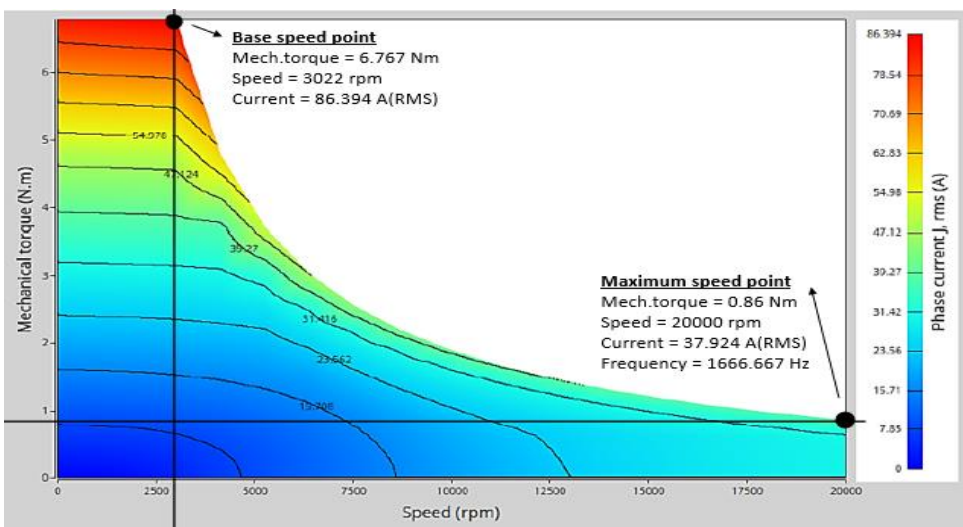


Figure 5 – Phase RMS current map of the motor in torque – angular speed area.

2.2. Component selection

After analysing the electrical characteristics of the motor, some power MOSFETs and gate drivers were compared with each other. The most important characteristics present in the datasheets of these devices are shown below and based on these parameters, it is easier to choose the most appropriate components for this project.

Starting from the Power MOSFETs choice, it is important that the power device satisfies the motor current requirements and which are strong enough to resist to the current spikes.

In the following tables, taken from the datasheets, the absolute maximum ratings regarding three different power MOSFETs are shown.

The three power devices are:

- **CSD18536KCS**
- **CSD19535KCS**
- **CSD19536KTT**

The first power MOSFET, CSD18536KCS, has the V_{DS} of 60V and it accepts a continuous drain current up to 200A. In the graph, however, it can be seen that the device also accepts higher currents for short duration pulse conditions. The graph represents the Safe Operating Area (SOA), the area where the voltage and current conditions over which the device can be expected to operate without self-damage.

Table 4 - Absolute maximum ratings from the CSD18536KCS datasheet [16].

$T_A = 25^\circ\text{C}$		VALUE	UNIT
V_{DS}	Drain-to-Source Voltage	60	V
V_{GS}	Gate-to-Source Voltage	± 20	V
I_D	Continuous Drain Current (Package limited)	200	A
	Continuous Drain Current (Silicon limited), $T_C = 25^\circ\text{C}$	349	
	Continuous Drain Current (Silicon limited), $T_C = 100^\circ\text{C}$	247	
I_{DM}	Pulsed Drain Current ⁽¹⁾	400	A
P_D	Power Dissipation	375	W
T_J, T_{stg}	Operating Junction and Storage Temperature Range	-55 to 175	$^\circ\text{C}$

(1) Max $R_{\theta JC} = 0.4^\circ\text{C/W}$, pulse duration $\leq 100\mu\text{s}$, duty cycle $\leq 1\%$.

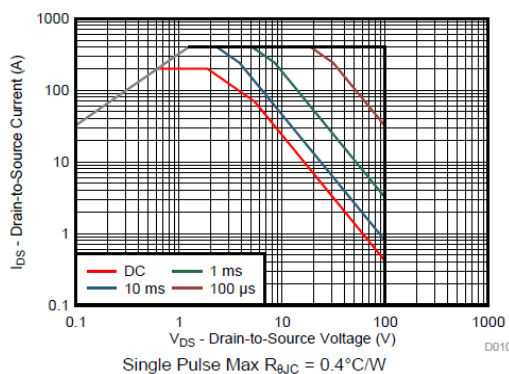


Figure 6 - Maximum safe operating area.

The absolute maximum ratings tables are also shown for the other two power MOSFETs, CSD19535KCS and CSD19536KTT.

The CSD19535KCS has a bigger V_{DS} value than the CSD18536KCS and a smaller value of the continuous drain current, in the table $V_{DS}=100V$ and $I_D=150A$.

For these devices the dynamic characteristics are shown, an important parameter is the gate charge gate to drain ($Q_{GD}=13nC$), used to calculate the gate driver current or the slew rate of the power device.

Table 5 - Absolute maximum ratings of the CSD19535KCS MOSFET, from the datasheet [15].

$T_A = 25^\circ C$		VALUE	UNIT
V_{DS}	Drain-to-Source Voltage	100	V
V_{GS}	Gate-to-Source Voltage	± 20	V
I_D	Continuous Drain Current (Package limited)	150	A
	Continuous Drain Current (Silicon limited), $T_C = 25^\circ C$	187	
	Continuous Drain Current (Silicon limited), $T_C = 100^\circ C$	133	
I_{DM}	Pulsed Drain Current ⁽¹⁾	300	A
P_D	Power Dissipation	375	W
T_J, T_{stg}	Operating Junction and Storage Temperature Range	-55 to 175	$^\circ C$

(1) Max $R_{\theta JC} = 0.5^\circ C/W$, pulse duration $\leq 100\mu s$, duty cycle $\leq 1\%$.

Table 6 - Main dynamic characteristics.

$T_A = 25^\circ C$		TYPICAL VALUE		UNIT
V_{DS}	Drain-to-Source Voltage	100		V
Q_G	Gate Charge Total (10V)	78		nC
Q_{GD}	Gate Charge Gate to Drain	13		nC
$R_{DS(on)}$	Drain-to-Source On Resistance	$V_{GS} = 6 V$	3.4	m Ω
		$V_{GS} = 10 V$	3.1	m Ω
$V_{GS(th)}$	Threshold Voltage	2.7		V

The best device is the last one, CSD19536KTT, because it has $V_{DS}=100V$ and $I_D=200$, so it is the most robust MOSFET. Q_{GD} is equal to 17 nC and other parameter which must be considered is the $R_{DS(on)}$, the drain to source on resistance, of 2 m Ω .

Table 7 - Absolute maximum ratings of the CSD19536KTT power MOSFET [14].

$T_A = 25^\circ C$		VALUE	UNIT
V_{DS}	Drain-to-Source Voltage	100	V
V_{GS}	Gate-to-Source Voltage	± 20	V
I_D	Continuous Drain Current (Package limited)	200	A
	Continuous Drain Current (Silicon limited), $T_C = 25^\circ C$	272	
	Continuous Drain Current (Silicon limited), $T_C = 100^\circ C$	192	
I_{DM}	Pulsed Drain Current ⁽¹⁾	400	A
P_D	Power Dissipation	375	W
T_J, T_{stg}	Operating Junction and Storage Temperature Range	-55 to 175	$^\circ C$

(1) Max $R_{\theta JC} = 0.4^\circ C/W$, pulse duration $\leq 100\mu s$, duty cycle $\leq 1\%$.

Table 8 - Main dynamic characteristics.

T _A = 25°C		TYPICAL VALUE		UNIT
V _{DS}	Drain-to-Source Voltage	100		V
Q _G	Gate Charge Total (10V)	118		nC
Q _{GD}	Gate Charge Gate to Drain	17		nC
R _{DS(on)}	Drain-to-Source On Resistance	V _{GS} = 6 V	2.2	mΩ
		V _{GS} = 10 V	2	mΩ
V _{GS(th)}	Threshold Voltage	2.5		V

At the end, the CSD19536KTT is selected for this project, this power device has been used in the simulation to verify that works properly. For completeness also other simulations using another power device have been done to compare the results (described in the next sections).

DRIVER PROBLEMS

The main and usual problem of the driver is the current limits, how much current is needed to give to the MOSFET gate or to be absorbed. In particular, this problem causes damage on the driver output pins that are connected to the external power MOSFETs.

Searching in the Texas Instruments forum, there are some discussions about the same problems. A possible reason that can be related to this problem concerns a specific parameter called I_{DRIVE} and how it is set. The I_{DRIVE} is an adjustable gate drive current that is incorporated in many smart gate drivers of TI products, specifically in many of the motor gate drivers to easily control the MOSFET slew rate [8], [7].

The goal of the correct I_{DRIVE} setting is to allow fast switching of the FET so that the resistive region of the FET is limited while also preventing ringing of the switch node and gate signals.

The first problem is that driving the gates too hard can damage the MOSFET, the gate driver or cause excess ringing and noise in the system. On the contrary, if this I_{DRIVE} setting is too low and not fully enhancing the power switches, the MOSFETs and the gate drivers may undergo unnecessary heating. To resolve this issue, this parameter can be increased one or two settings higher until better enhancement is reached but not so much that ringing is caused.

Some considerations can be done starting by a simplified equation used to find the slew rate of the MOSFET V_{DS} (drain-to-source voltage):

$$SR_{DS} = I_{DRIVE} \times \frac{V_{DS}}{Q_{GD}}$$

Where:

- SR_{DS} = slew rate of the drain to source voltage of the power MOSFET, in seconds
- I_{DRIVE} = current sourced to or sunk out of the gate, in amps
- V_{DS} = voltage difference between the MOSFET drain voltage and source, in volts

- Q_{GD} = inherent gate-to-drain charge for the MOSFET, in coulombs

According to previous equation, a high I_{DRIVE} and a small Q_{GD} results in a very fast slew rate, as V_{DRAIN} is usually fixed in a motor control system, unless the system supply voltage is specifically designed to change, but this is not the case.

So, it would seem that the slew rate could be increased to very high values in order to reduce the switching losses in the MOSFETs, but it is not a good idea setting the slew rate as high as possible because there are adverse effects in a high-power system.

In fact, all the current flowing through the MOSFETs increases their inherent capacitive coupling and the effects of parasitic LC resonance, causing a more quickly V_{DS} voltage transition.

As shown in the following figure, the high-frequency component of the rising edge of the gate signal (V_{GHx}) and, more importantly, the rising V_{DS} signal going through the Miller region (where V_{DS} drops and V_{GS} remains constant), causes current to flow through the intrinsic capacitors of the other MOSFET (in the figure the low side device). This signal couples through the inherent gate-to-drain (C_{GD}) or gate-to-source (C_{GS}) capacitor because capacitors have lower impedance at higher frequencies.

The big problem is that if these coupled signals are high enough, they can exceed absolute maximum ratings of the motor driver or turn on the low and high-side MOSFETs within one phase (at the same time) and this causes a shoot-through condition as current bypasses the motor and flows through the direct path from V_{DRAIN} to ground.

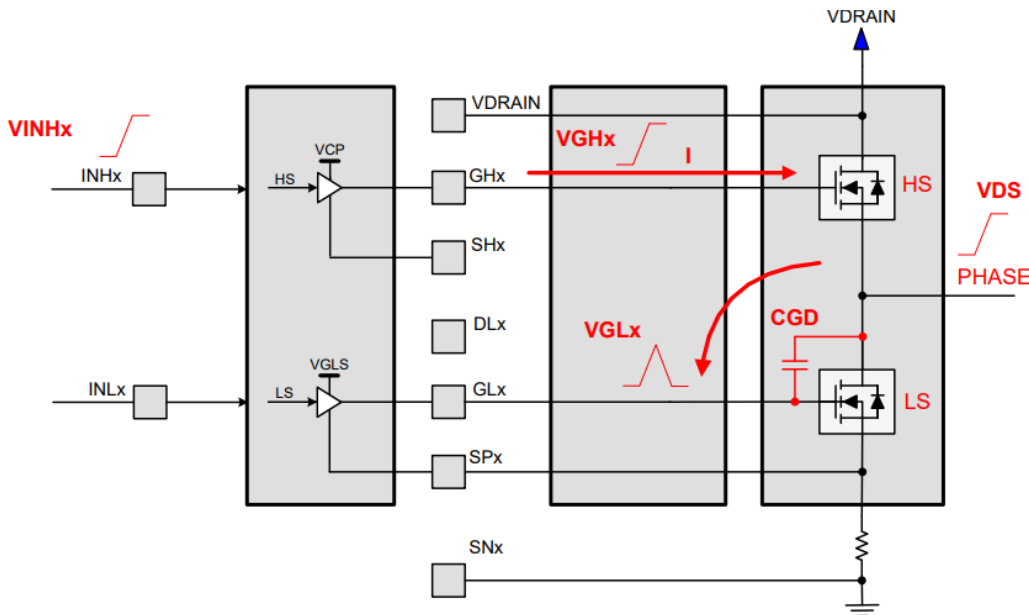


Figure 7 - Shoot through condition, inductive spiking and coupling from switching on MOSFET.

- Estimate needed VDS rise and fall time (for many high-power systems, rise and fall times between 100 ns to 300 ns are a good starting point as a general guideline)
- Alternatively, the designer can rearrange the previous equation to get the equation in terms of gate drive current (I_{DRIVE}) instead of V_{DS} slew rate (SR_{DS}) where 25 V/ μ s to 100 V/ μ s is acceptable as general input:

$$I_{DRIVE} = \frac{Q_{GD}}{t_{RiseFall}}$$

Where:

- I_{DRIVE} = current sourced to or sunk out of the gate, in amps
- $t_{RiseFall}$ = equivalent rise or fall time for the V_{DS} (not V_{GS}), in seconds
- Q_{GD} = inherent gate-to-drain charge of the MOSFET, in coulombs

For the case of the CSD19536KTT, $Q_{GD} = 17$ nC and we can use the general guidelines to put 100 ns into the rise and fall time.

(Note, some designers like to make the fall time two times faster than the rise time)

$$I_{DRIVE} = \frac{17 \text{ nC}}{100 \text{ ns}} = 170 \text{ mA}$$

The DRV835x family does not have an IDRIVE setting of exactly 170 mA, but it does have lower options of 150 mA or 100 mA for source current and 100 mA for sink current.

Source refers to the current taken from the gate voltage supply and pushed into the FET, which corresponds with the rise time; and sink refers to the rate at which charge is pulled from the gate of the FET and pushed to the source of the FET, which corresponds with the fall time. In the case where the rise and fall time is 300 ns, the same equation can be used:

$$I_{DRIVE} = \frac{17 \text{ nC}}{300 \text{ ns}} = 56 \text{ mA}$$

Using the DRV835x family again, choose 50 mA for the source current but the smallest sink current is 100 mA.

This is a perfect example for adding a gate resistor to adjust the sink and source current, to obtain a more precise value respect to the current settings available in the gate driver used in this application.

Remember, we are merely using a starting gate drive current that was calculated with a safe general guideline. This is a first order equation and does not exactly match what is seen in the real system, but the goal is to get within a reasonable starting point.

This is why we round down if the device does not have an exact selection, to make the equivalent rise or fall time to be longer than the calculated value. Designers are expected to increase or decrease this number after testing.

Selecting the best gate driver between DRV8323 and UCC27282-Q1 and motivations:

The first driver analysed is the DRV8323. The device provides three half bridge gate drivers, each capable of driving high side and low side N-channel power MOSFETs.

It has a smart gate drive architecture that supports peak gate drive currents up to 1A source and 2A sink. The DRV8323 supports a wide input supply range of 6 to 60V.

This smart gate driver implements adjustable gate drive current to control the MOSFET V_{DS} slew rates. The I_{DRIVE} component lets the driver dynamically switch between gate drive currents either through a register setting on SPI devices (the Serial Peripheral Interface included in the component structure), or the I_{DRIVE} pin on hardware interface devices (depending on the DRV8323 versions).

As explained in the previous section regarding driver problems, it is very important to set the I_{DRIVE} parameter in the SPI registers and it is not very easy to do it in a good way.

Another important parameter which is analysed in the next simulation sections is the propagation delay of this gate driver that is 150ns, and this value is not so small.

For all these considerations another device has been proposed. The second component is a gate driver that, differently from the DRV832x family, is not a smart gate driver.

The UCC27282-Q1 is a robust N-channel MOSFET driver with a maximum switch node (HS pin) voltage rating of 100V (bigger than 60V of the first driver). It allows to control two power MOSFETs in half-bridge configuration. The device implements the cross-conduction protection functionality.

This gate driver is able to handle up to 3A peak source and sink currents (the DRV8323 has lower maximum peak currents) along with low pull-up and pulldown resistors and therefore it can drive large power MOSFETs with minimum switching losses during the transition of the MOSFET Miller plateau.

The last but very important difference from the DRV8323 is the propagation delay parameter. The UCC27282-Q1 has a typical propagation delay of 16 ns which is much lower than the other driver value (150 ns) and it has a rise time of 12 ns and a fall time of 10 ns which are excellent values.

In the next sessions some simulations using these two different gate drivers and some power devices are shown and looking at the currents graphs it is possible to verify the differences in behavior of the various devices listed.

2.3. Simulink model (gate driver - power MOSFET - battery load)

It is very important to test a simple circuit to have a general idea of the behaviour of the gate driver and the power MOSFET which can be used for the final inverter.

Simulink is very useful to simulate a simple system like this reported in the following figure.

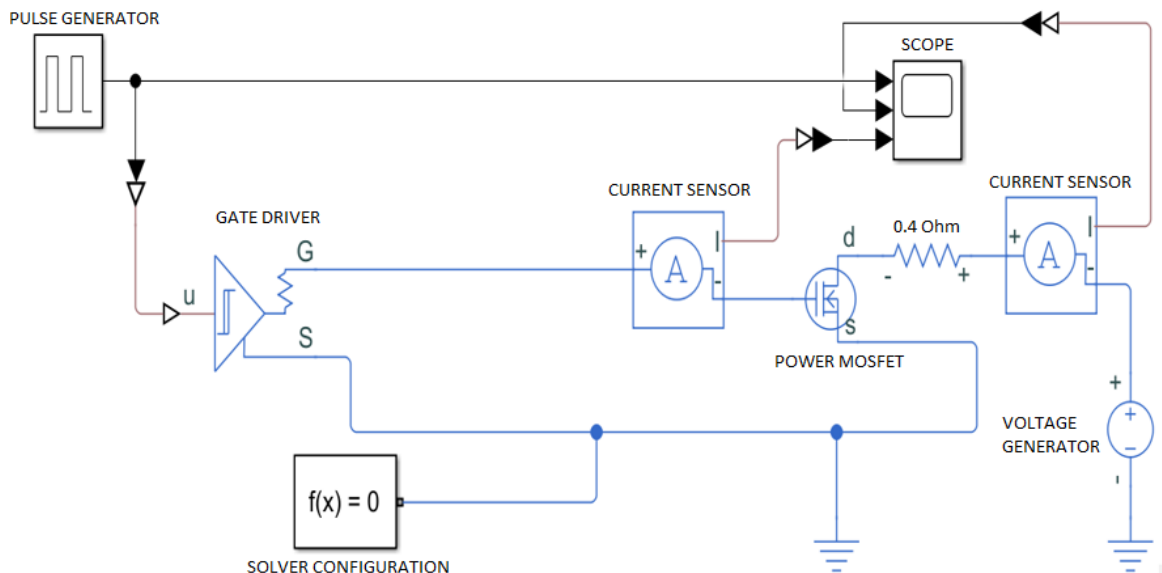


Figure 9 - Simulink scheme of gate driver - power MOSFET system.

For this scheme it is used a powerful tool called Simscape.

Simscape™ enables any user to rapidly create models of physical systems within the Simulink environment. In this case there is a Simscape block for the gate driver, the MOSFET and a voltage generator (battery) with a series resistor connected to the drain (a simple way to simulate a motor model).

It is important to check the currents flowing in the circuit, adding two current sensors for the gate driver output current and the drain current. Obviously, the input of the driver is a pulse generator which has the role of switching the MOSFET and so the motor phase.

A scope is put see all the signals which is important for the simulation. There are also other blocks like the solver configuration ($f(x) = 0$) and converters (in the figure the blocks with the double arrow) to convert a Simulink signal to a physical signal (Simscape) and vice versa.

The initial parameters of each device:

Since the switching frequency of the final control system is 20 kHz, the pulse generator period is $T = 1/20 \text{ kHz} = 50 \mu\text{s}$ and the duty cycle is 50 %.

Instead for the load it is used a voltage generator with nominal voltage = 48 V and a series resistor in order to have a maximum load current of 120 A to evaluate the worst case. Resistor value = $48V/120 A = 0.4 \Omega$.

Then, the block parameters of the gate driver and the MOSFET must be set.

Using the datasheet of the power device, the main parameters of the relative block must be set:

Table 9 - Main parameters from CSD88599Q5DC datasheet [13].

MOSFET SPECIFICATIONS (CSD88599Q5DC)		
Drain-Source on resistance, $R_{DS(on)}$	1.7	mΩ
Drain current, I_{DS} , for $R_{DS(on)}$	30	A
Gate-Source voltage, V_{GS} , for $R_{DS(on)}$	10	V
Gate-Source threshold voltage, V_{th}	2	V
Measurement temperature	25	°C
Input capacitance, C_{iss}	3720	pF
Reverse transfer capacitance, C_{rss}	12	pF
Output capacitance, C_{oss}	670	pF

The propagation delay (t_{PD}), INHx/INLx to GHx/GLx transition, is in the DRV832x datasheet.

The gate driver block is set using these parameters:

Table 10 - Gate Driver block parameters.

Input Logic		
Logic 1 input value	0.7	
Logic 0 input value	0.3	
Outputs		
On-state gate-source voltage	4.0	V
Off-state gate-source voltage	0.0	V
Timing		
Propagation delay (logic 0 -> logic 1)	150	ns
Propagation delay (logic 1 -> logic 0)	150	ns
Dynamics		
Parametrization	Output impedance	
On-state gate drive resistance	eps	Ohm
Off-state gate drive resistance	eps	Ohm

2.4. First simulation using the driver and the MOSFET initially chosen

In the first simulation it has been used the values related to the DRV8323 gate driver and CSD88599Q5DC power MOSFET. As it shown in the previous Simulink model, the gate driver output is directly connected to the power FET (no resistance between gate driver output and gate of the MOSFET).

Starting the simulation, the results can be analysed thanks to the current sensors and the trend of the current signals can be checked opening the scope block.

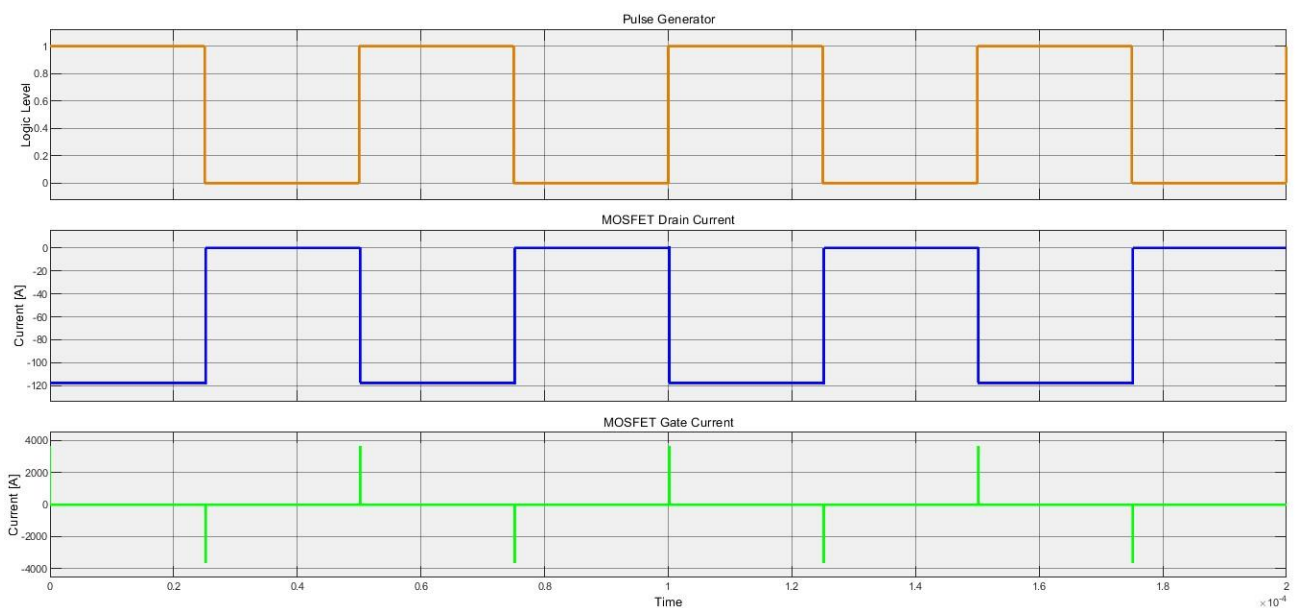


Figure 10 - Simulink scope, first simulation.

In the third graph it can be seen the saturation of the MOSFET gate current, more precisely this is the limit of the gate driver output current. The value is greater than 3000 A and for sure is not a realistic situation, remember that the DRV8323 supports peak source currents up to 1 A and peak sink currents up to 2 A.

If transitions are zoomed, the gate driver propagation delay is more visible and, measuring on the time axis, it can be verified the value of 150 ns set before.

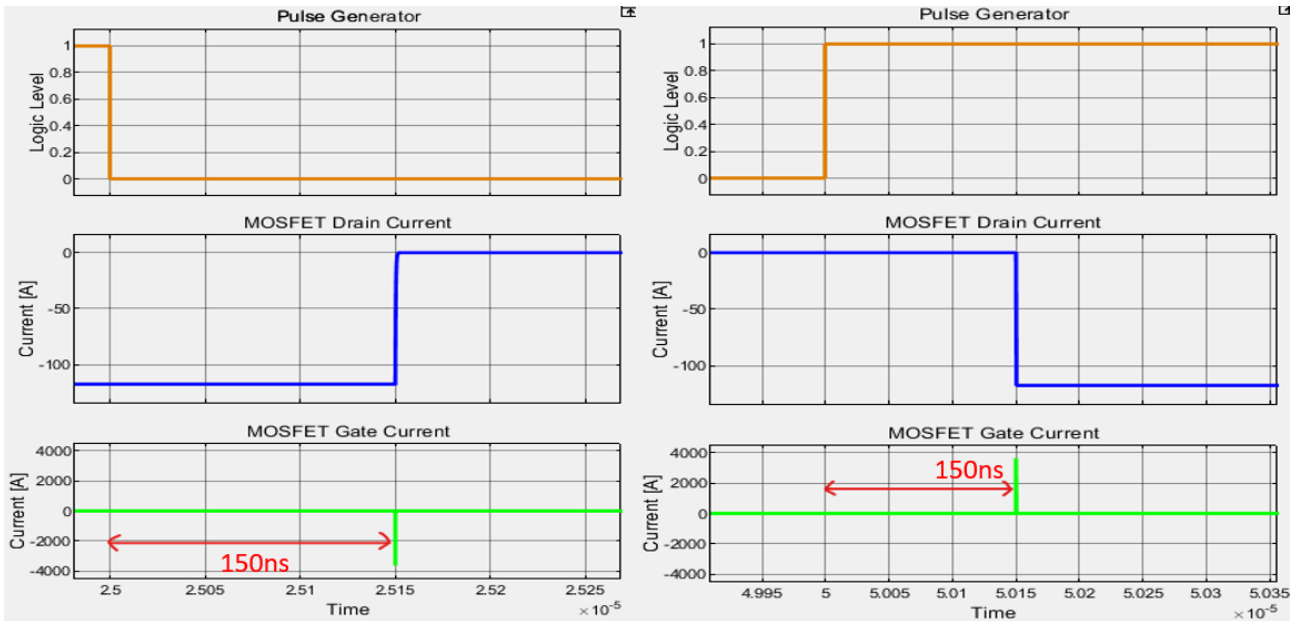


Figure 11 - First simulation (zoom, driver propagation delay).

If the second graph is zoomed, the rise and fall times of the MOSFET can be calculated.

In this first case the current that flows in the MOSFET is very high, so the transitions are too fast, 1 ns for the rise time and 350 ps for the fall time.

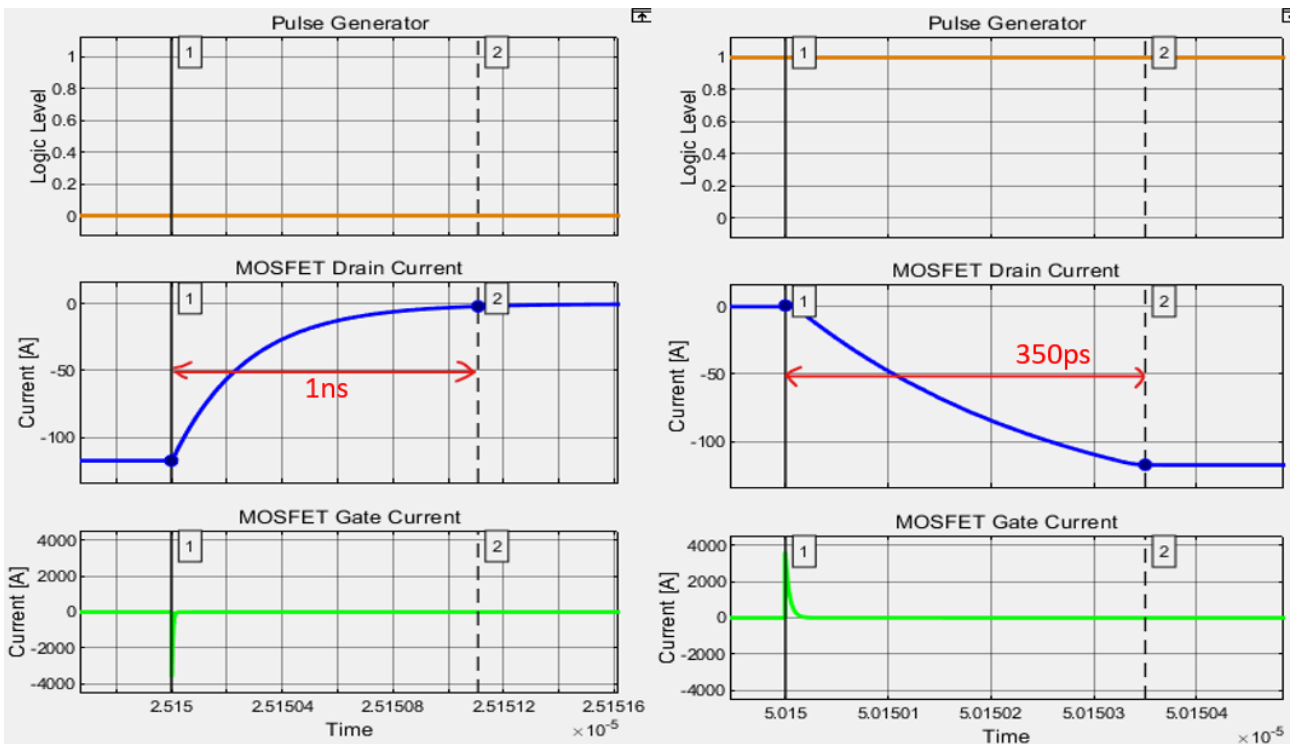


Figure 12 - First simulation (zoom, rise and fall time).

The currents flowing from the driver to the MOSFET can be decreased adding two resistances of $5\ \Omega$ and one diode between gate driver output and gate of the MOSFET.

Info on the diode: forward voltage of $0.6\ \text{V}$, on resistance of $0.3\ \Omega$ and off conductance of $1 \times 10^{-8}\ \text{S}$ (or $1/\Omega$).

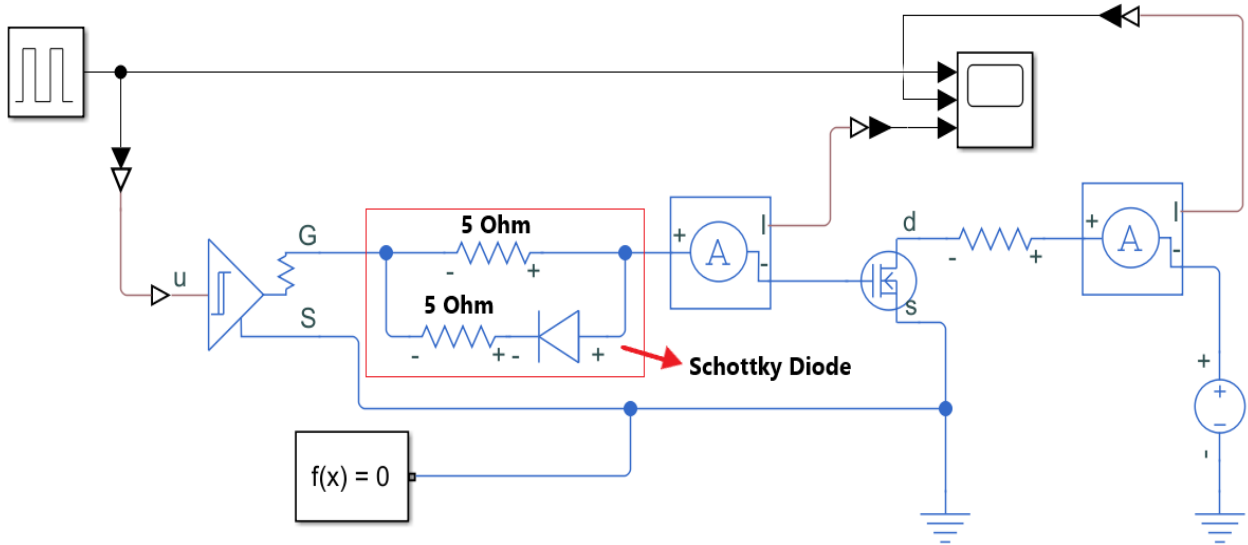


Figure 13 - Simulink scheme, adding two $5\ \text{Ohm}$ resistors and one diode between the driver and the MOSFET.

Zooming on the transitions the driver propagation delay is always $150\ \text{ns}$.

Now the maximum sink and source currents are within the limits (sink current is $1.4\ \text{A}$, which is smaller than $2\ \text{A}$, and source = $0.8\ \text{A} < 1\ \text{A}$), but the rise and fall times are bigger, the transitions are slower and, therefore, there is an increase in the total propagation delay.

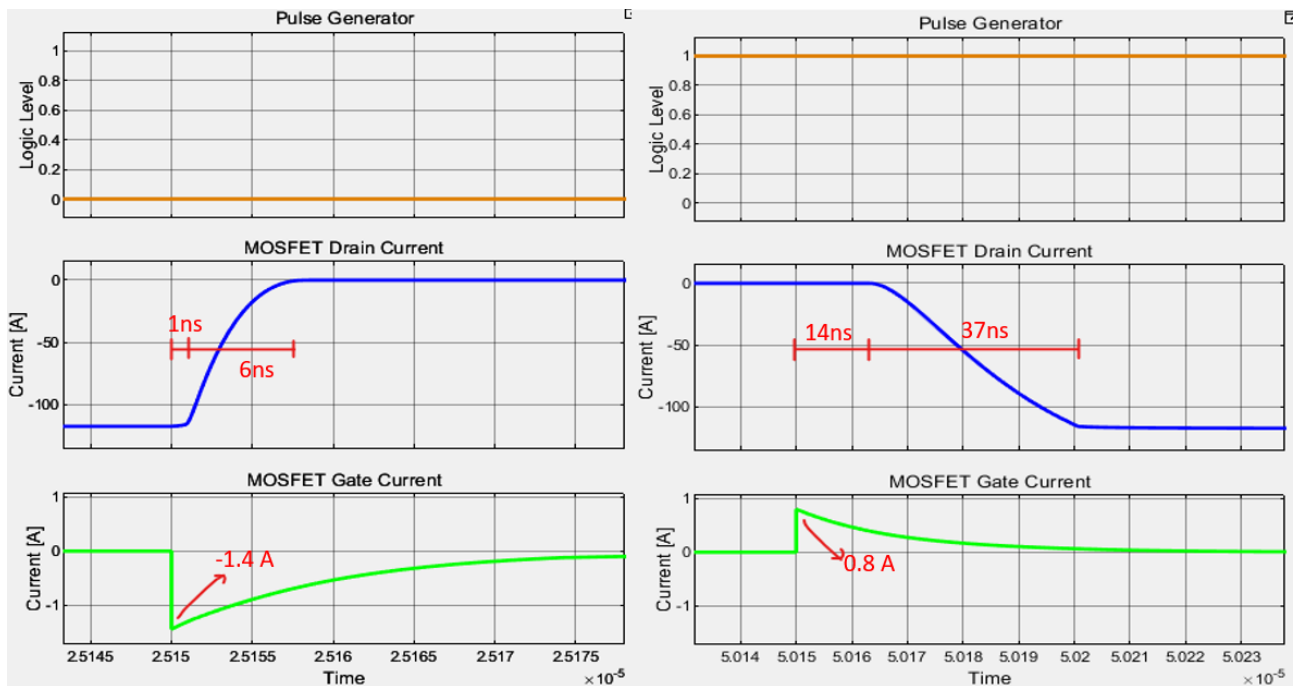


Figure 14 - Second simulation, within the resistances and the diode.

Just for example the 5 Ω resistors can be replaced by two 10 Ω resistors and the changes is shown in the figure:

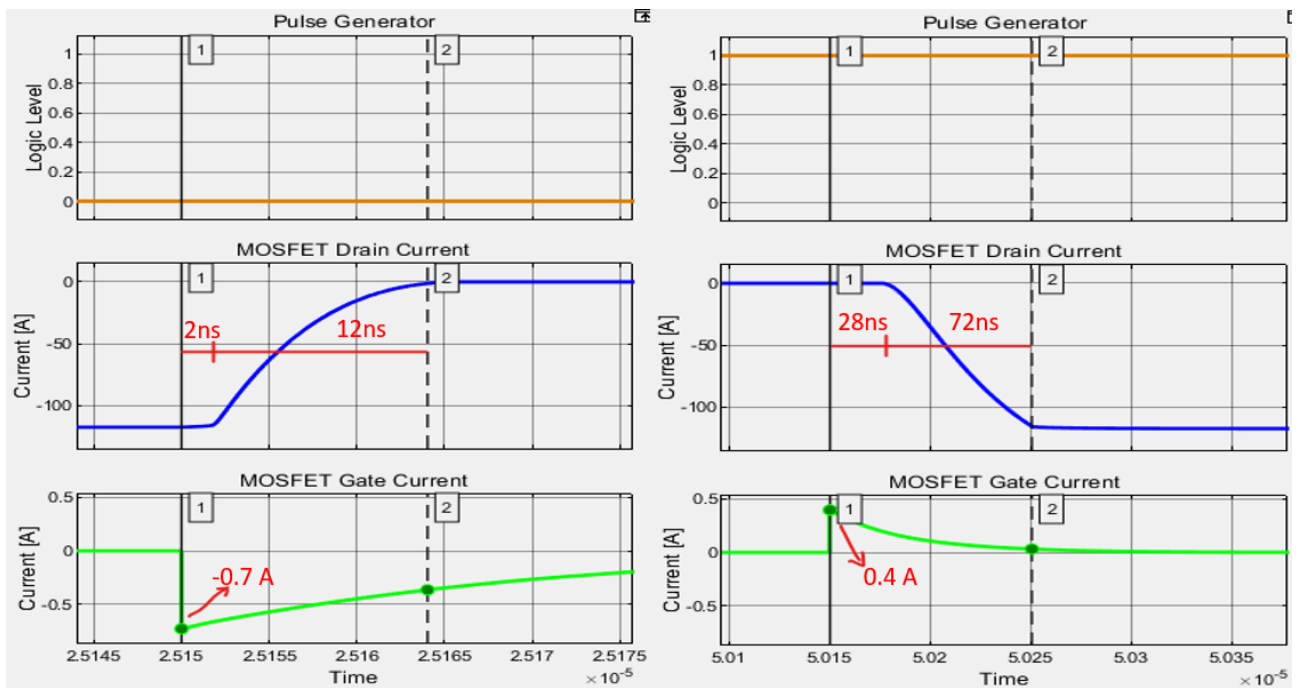


Figure 15 - Second simulation, with 10 Ohm resistors.

It is evident that the currents are smaller (halved) and accordingly the delays are bigger (doubled).

2.5. Second simulation using the new driver and MOSFET

The simulation is executed using other type of MOSFET, the CSD19536KTT. The main parameters are reported in the table.

Table 11 - Main MOSFET block parameters from CSD19536KTT datasheet.

MOSFET SPECIFICATIONS (CSD19536KTT)		
Drain-Source on resistance, $R_{DS(on)}$	2	m Ω
Drain current, I_{DS} , for $R_{DS(on)}$	100	A
Gate-Source voltage, V_{GS} , for $R_{DS(on)}$	10	V
Gate-Source threshold voltage, V_{th}	2.5	V
Measurement temperature	25	$^{\circ}\text{C}$
Input capacitance, C_{iss}	9250	pF
Reverse transfer capacitance, C_{rss}	47	pF
Output capacitance, C_{oss}	1820	pF

In this simulation two 5 Ω resistances are used and the results are quite like the previous simulation with the other power device. The rise and fall times are so close to the previous ones, instead the maximum currents are higher, but they respect the driver limits.

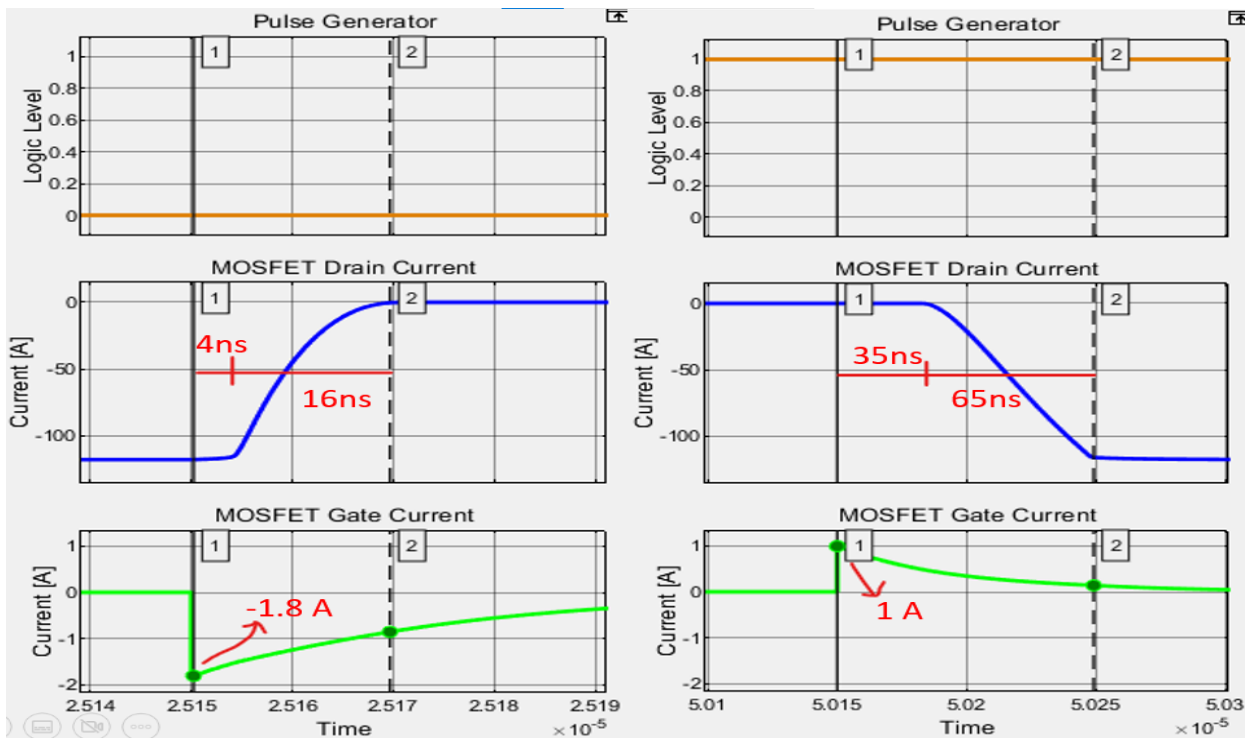


Figure 16 - Third simulation, CSD19536KTT MOSFET and 5 Ohm resistors.

Another simulation shows the device behaviour with 10 Ω resistors, resulting in smaller currents and slower transitions.

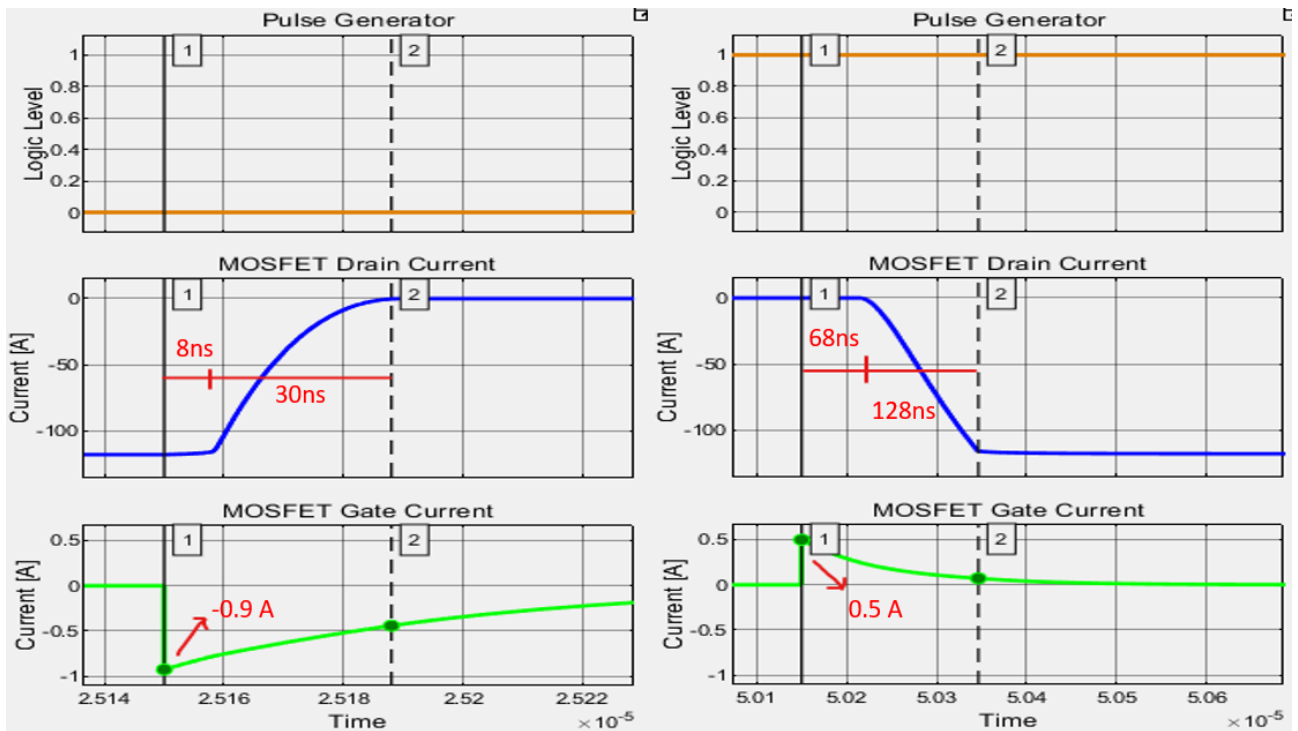


Figure 17 - Third simulation, CSD19536KTT MOSFET and 10 Ohm resistors.

Now the DRV8323 gate driver is replaced by the UCC27282-Q1 [12]. This gate driver allows more sink and source peak current up to 3 A. But most of all it has a low propagation delay, as it is described in the datasheet. Now the delay is 16 ns, which is much lower than the previous driver delay of 150 ns. The output rise and fall time are respectively 12 and 10 ns, with a load capacitance of 1800 pF.

So, the block parameters must be replaced with the new ones, the rise and fall times are also set accordingly with the datasheet values (in the previous figure).

Table 12 - Main driver block parameters.

Timing		
Propagation delay (logic 0 -> logic 1)	16	ns
Propagation delay (logic 1 -> logic 0)	16	ns
Dynamics		
Parametrization	Rise and fall times	
Rise time	12	ns
Fall time	10	ns
Load capacitance for rise and fall times	1800	pF

Two new simulations have been executed with this new gate driver, one with the CSD88599Q5DC and the other using the CSD19536KTT. In both simulations two 5 Ω resistors and one diode are added as before.

The results are described in detail in the next section.

2.6. Graphic representation and tables with delays measurement

The following figures describe the graphical behaviour of the two last simulations, both with the UCC27282-Q1 gate driver, the first using the CSD88599Q5DC component and the second with the CSD19536KTT power device.

- Power device used: CSD88599Q5DC.

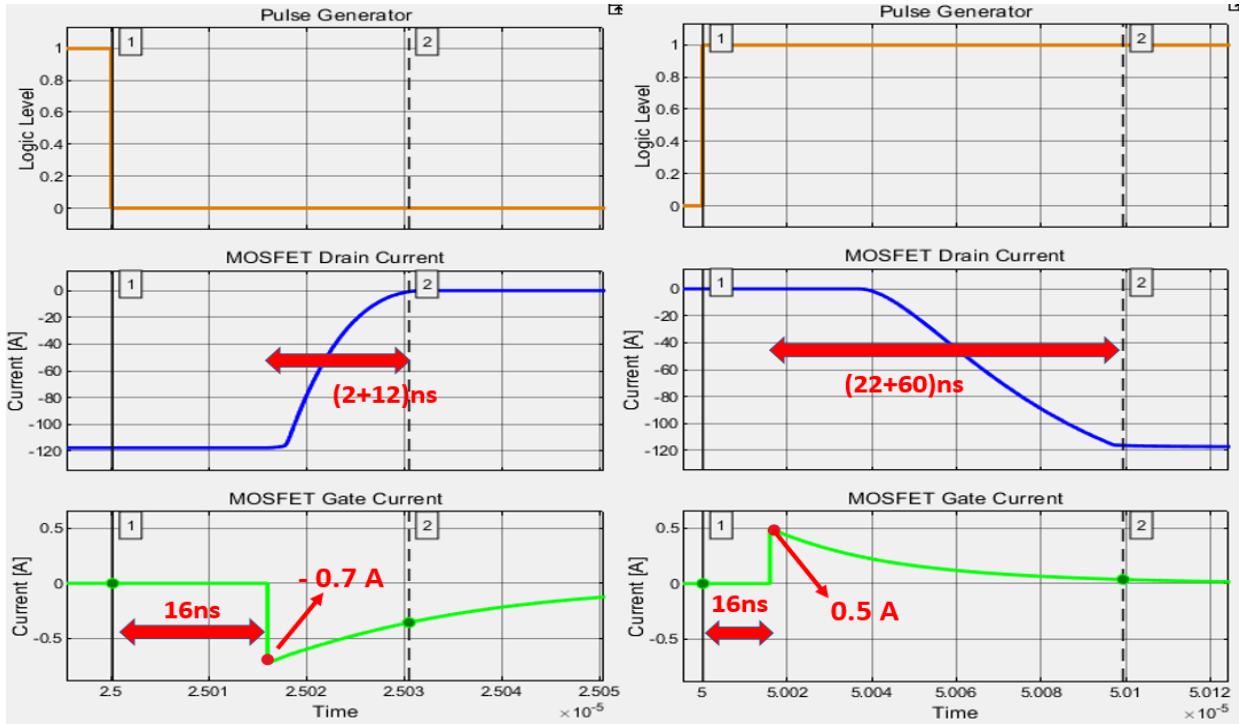


Figure 18 - Fourth simulation, UCC27282-Q1 + CSD88599Q5DC + 5 Ohm resistors.

- Power device used: CSD19536KTT.

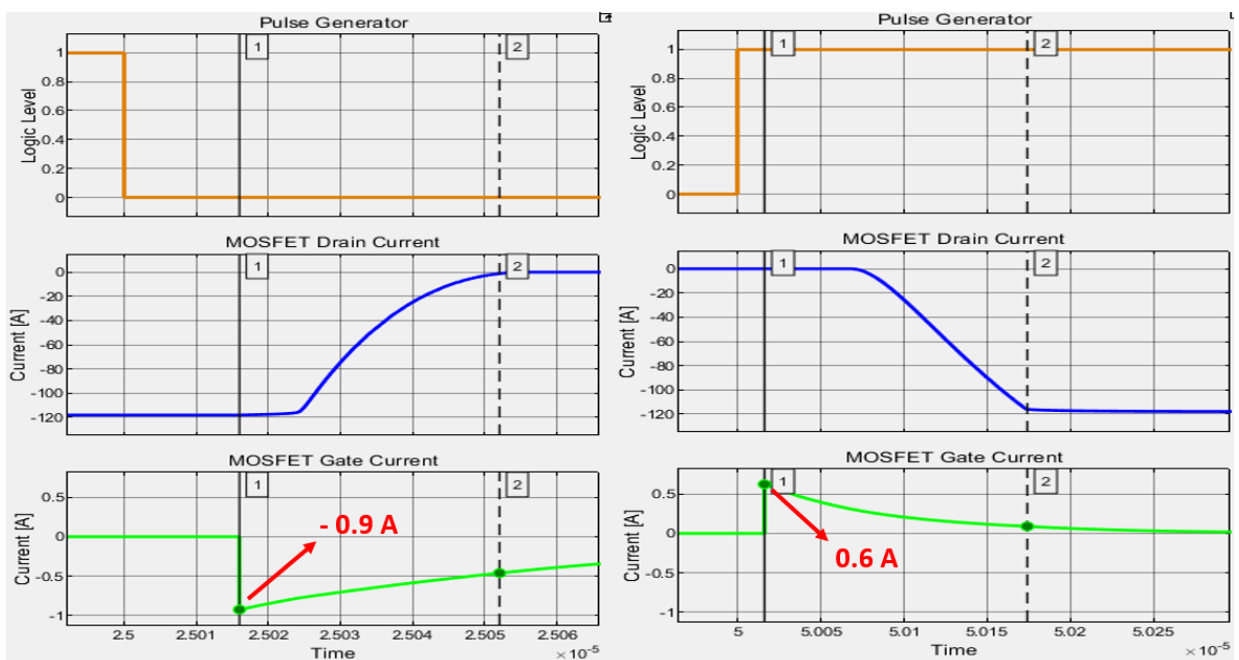


Figure 19 - Fourth simulation, UCC27282-Q1 + CSD19536KTT + 5 Ohm resistors.

The Simulink scopes show the MOSFET gate current is very low respect to the maximum current that the gate driver is able to source or to sink, the peak currents don't exceed 1A and this is a good value because the driver accepts up to 3A.

Resuming tables with all delay measurements and some final comments.

The first table reports the time delays when the DRV8323 gate driver is used.

In the first column there is a description of the MOSFET and configuration used.

Table 13 - Time delays using the DRV8323 smart gate driver.

DRV8323	Delay before L-H transition	Rise time	Total delay (L-H)	Delay before H-L transition	Fall time	Total delay (H-L)	Gate driver propagation delay	Total delay during one period
CSD88599Q5DC with 5Ω resistors	1ns	6ns	7ns	14ns	37ns	51ns	150ns	358ns
CSD88599Q5DC with 10Ω resistors	2ns	12ns	14ns	28ns	72ns	100ns	150ns	414ns
CSD19536KTT with 5Ω resistors	4ns	16ns	20ns	35ns	65ns	100ns	150ns	420ns
CSD19536KTT with 10Ω resistors	8ns	30ns	38ns	68ns	128ns	196ns	150ns	534ns

As the table shows, the second device is slower than the first and if the resistors value are increased there is a time delay increase too.

The second table describes the Simulink model with the UCC27282-Q1 gate driver.

Table 14 - Time delays using the UCC27282-Q1 gate driver.

UCC27282-Q1	Delay before L-H transition	Rise time	Total delay (L-H)	Delay before H-L transition	Fall time	Total delay (H-L)	Gate driver propagation delay	Total delay during one period
CSD88599Q5DC with 5Ω resistors	4ns	12ns	14ns	22ns	60ns	82ns	16ns	128ns
CSD19536KTT with 5Ω resistors	8ns	28ns	36ns	55ns	103ns	158ns	16ns	236ns

The CSD88599Q5DC is faster than the second device, the total delay during one period is about half of the other value (236 ns). But the CSD19536KTT power MOSFET is more appropriate for this application because it allows to manage high currents and voltages (see in the absolute maximum ratings of the CSD19536KTT datasheet, table shown in the previous sections).

Final considerations

Moreover, having a total delay of 236 ns during one single period is not a problem because the total switching period is 50000 ns (1/20 kHz) and, although delay values of 500 ns are permitted (1% on the total T_s), the total delay is sufficiently smaller than this threshold.

The final choice is the CSD1936KTT power MOSFET and the UCC27282-Q1 gate driver, adding between these devices the diode and the two resistors of 5 Ω .

3. Results

3.1. The final PCB, with design comments

After the problems analysis, the devices choice and the final validation through simulation, all these design phases must be considered to produce a complete PCB (Printed Circuit Board) which represents the final inverter to be connected to the electric motor.

The software used to produce this printed circuit is KiCad.

KiCad is an open-source suite which allows you to draw electrical schematics and to translate them into printed circuit boards.

In the electrical schematic section, an electrical symbol must be assigned to each component used in the project and all the symbols must be connected together as well as possible. When all the components have been placed and all the connections have been checked, the printed circuit can be designed.

The first thing to do is to assign a footprint to each symbol of the schematic. When all the devices have an assigned footprint the PCB design can start.

The most important two phases are the component placing and the tracks routing.

The components must be placed in the PCB in the best way following some rules described below. After the components have been placed, they must be connected drawing tracks and also in this phase some design rules must be considered to avoid problems and damages.

This is the total project composed by three subsystems:

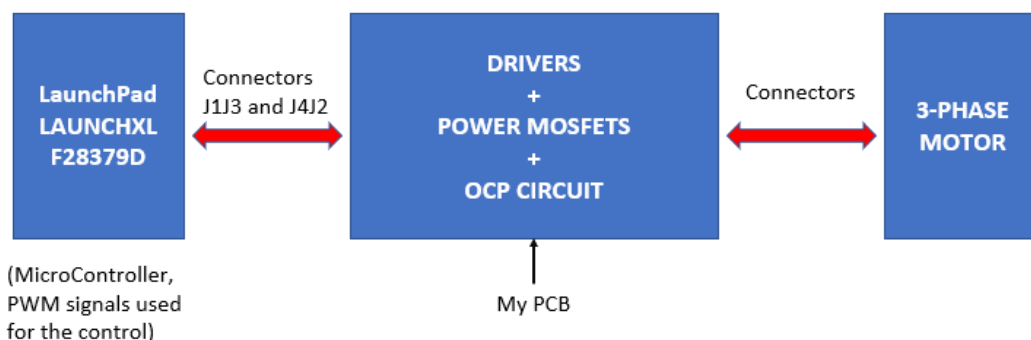


Figure 20 - Overall system with main connections between PCB and external components.

In the next figure it is shown the general schematic implemented in KiCad, each component has an associated symbol and, as it is explained after, each symbol will be assigned a footprint, who it will be placed in the final PCB.

The schematic is also important because all the connections are represented.

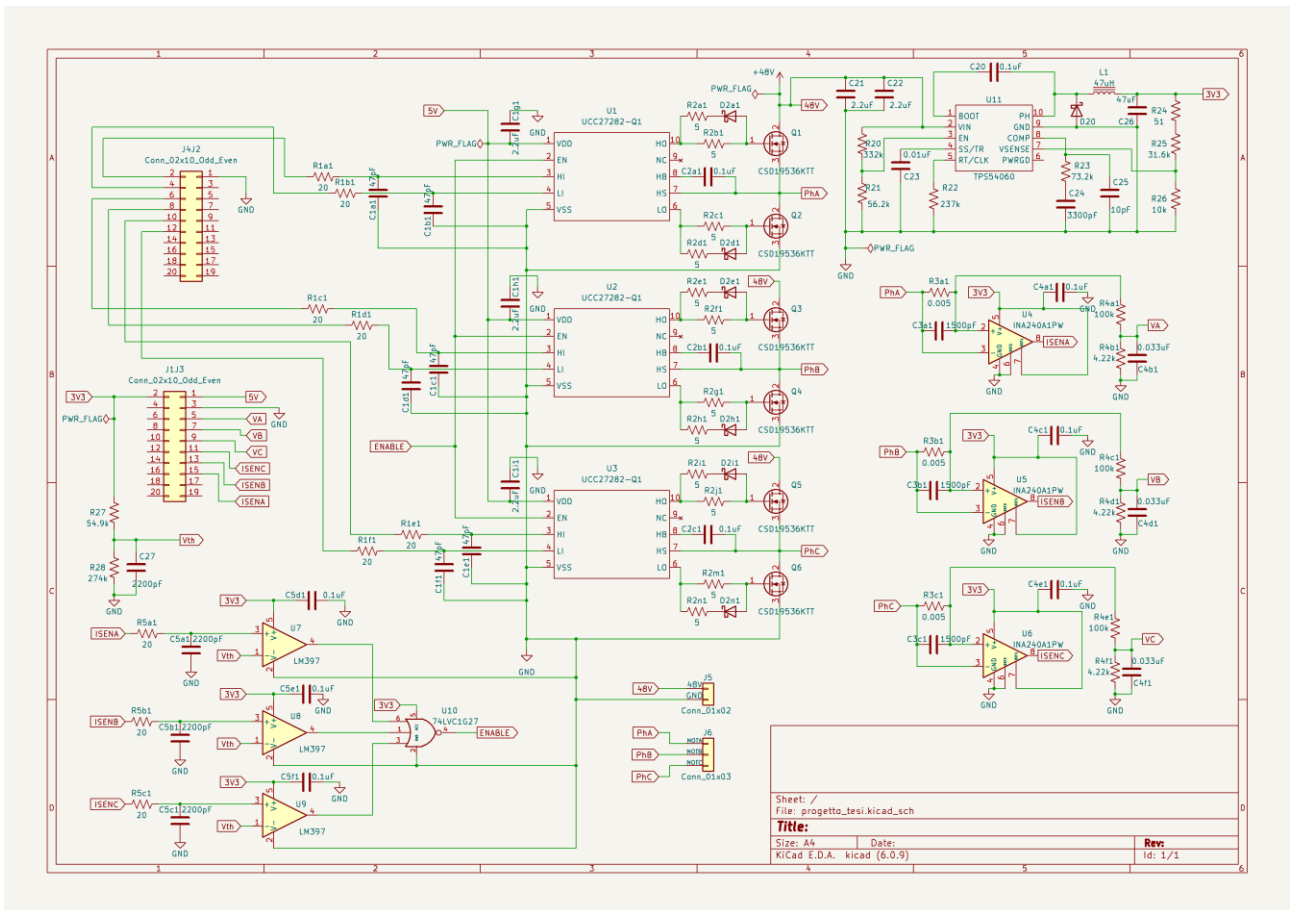


Figure 21 - The general circuit with all the symbols and their connections, screen taken from schematic editor in KiCad.

Now, all the circuit is divided into more subcircuits to analyse the components used in each block and their functions.

First the connection between the Launchpad and the first part of the inverter is shown, where three drivers are present (one for each motor phase).

In the figure below It is shown the schematic part where the two launchpad connectors are linked to the driver inputs, using also low pass filters to clean the signals generated by the microcontroller.

The two connectors of the microcontroller, called J4J2 and J1J3, are composed by 2x10 pins. More precisely the first 6 pins of J4 are used to transmit the PWM signals to the HI and LI inputs of the gate drivers.

Instead, the J1J3 connector is used for the motor voltage and current measurements.

The low pass filters used are composed by a 20-ohm resistor and a 47-pF capacitor.

The UCC27282-Q1 offers both negative input voltage handling capability and wide input threshold hysteresis. If these features are not enough, then the application might need an input filter. Small filter such as 20-Ω resistor and 47-pF capacitor might be sufficient to filter noise at the inputs of the gate driver device. The time constant of the filters can be calculated: $\tau = R \times C = 0.940 \text{ ns}$.

It needs a VDD bypass capacitor about some micro farads to eliminate the noise on the supply pin and more stable. In this case a proper value of the capacitor could be 2.2 μF , must be ceramic types with X7R dielectric or better and voltage of 25 V (tolerance of 5% or better 1% if possible).

Also place a small size, 0402, low value, 1 nF, capacitor to filter high frequency noise, in parallel with main bypass capacitor.

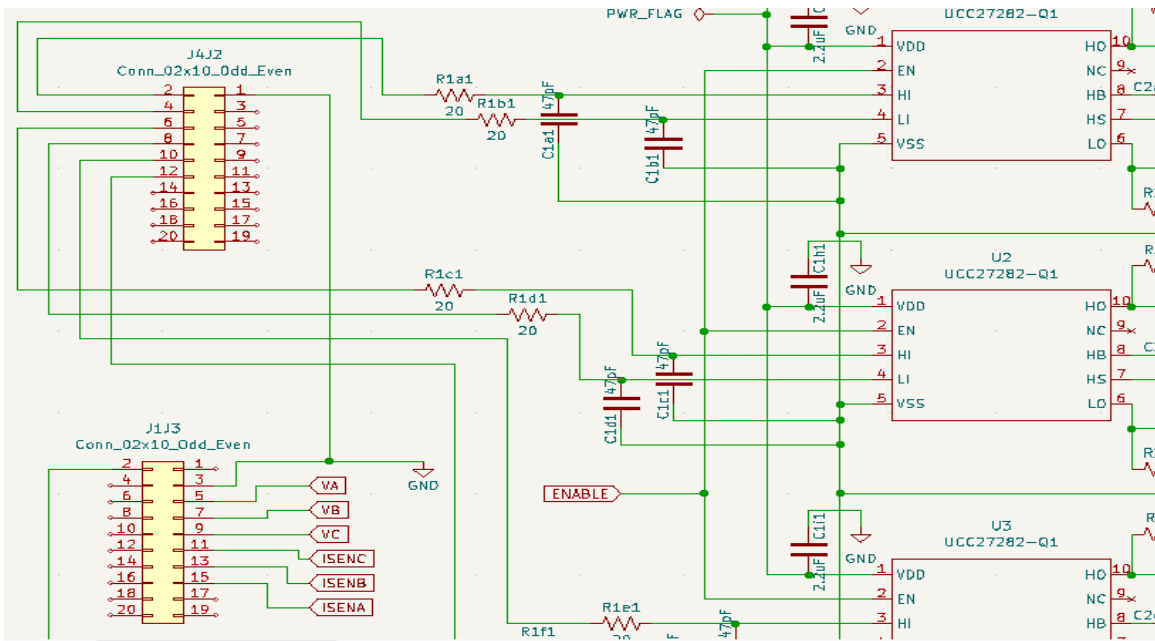


Figure 22 - Zoom on the connection between the LaunchPad connectors and the gate drivers.

Other important connections to point out are between drivers and power switches.

The driver has two outputs HO (high output pin) and LO (low output pin) which drive the high side and low side MOSFET respectively.

As said in the previous chapters, to control the slew rate of the applied gate voltage and reduce the peak current applied to the gate of the FET, is an optimal solution adding 5 Ω resistors (one for the sink current and the other for the source one) and a Schottky diode.

Furthermore, it is important to place one bootstrap capacitor (between HB and HS driver pins) of 0.1 μF , 25 V, 5% tolerance. Also, this capacitor must be ceramic types with X7R dielectric and it is always a good standard place a small size (0402) capacitor of 1 nF to filter high frequency noise, in parallel with main bootstrap capacitor.

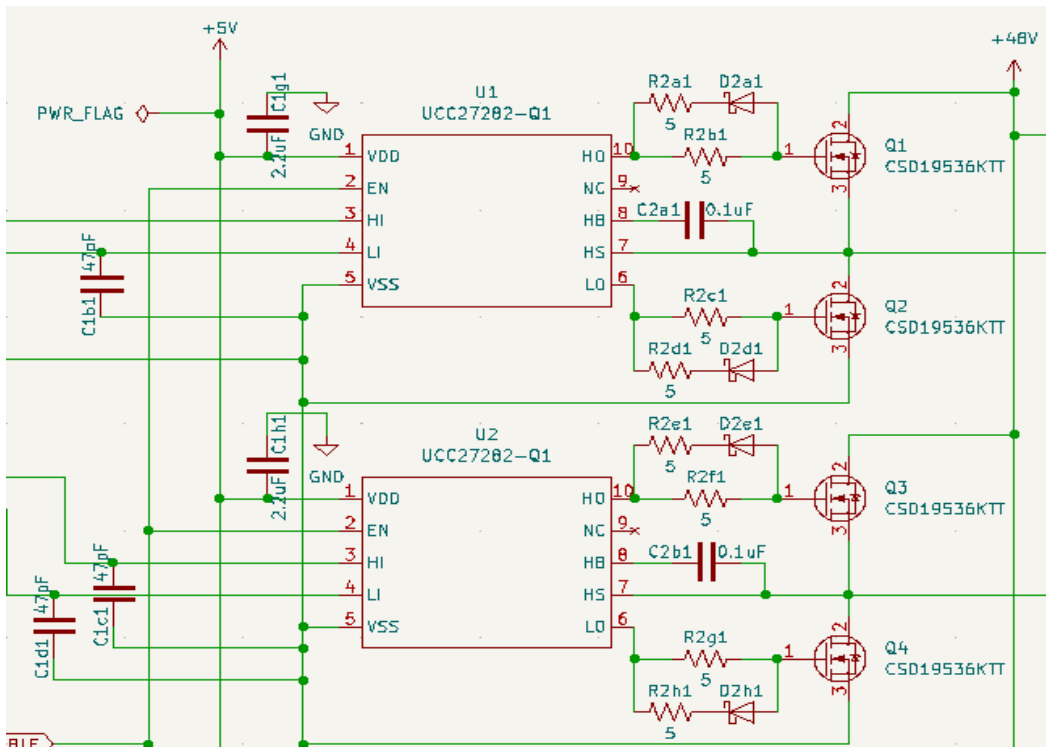


Figure 23 - Zoom on the connection between the gate drivers and the power MOSFETs.

Phase current/voltage sense:

This circuit is used to measure the motor phase currents. The main device is a current sense resistor, specifically an ultra-low sensing resistance of 5 mΩ.

Other important data of this resistor are:

Tolerance = 1%

Power rating = 0.25 W

Temperature coefficient = 150 ppm/°C

Operating temperature range: -55 to +170 °C

Footprint info: chip size = 0402, SMD/SMT

For this application is used the INA240A1PW, a bidirectional and ultra-precise current sense amplifier with enhanced PWM rejection.

Then, it is useful to add a 1500-pF capacitor in parallel to the sense resistor, which is the INA240A1PW input capacitor. Another bypass capacitors of 0.1 µF connected to the Vcc pin of the amplifier.

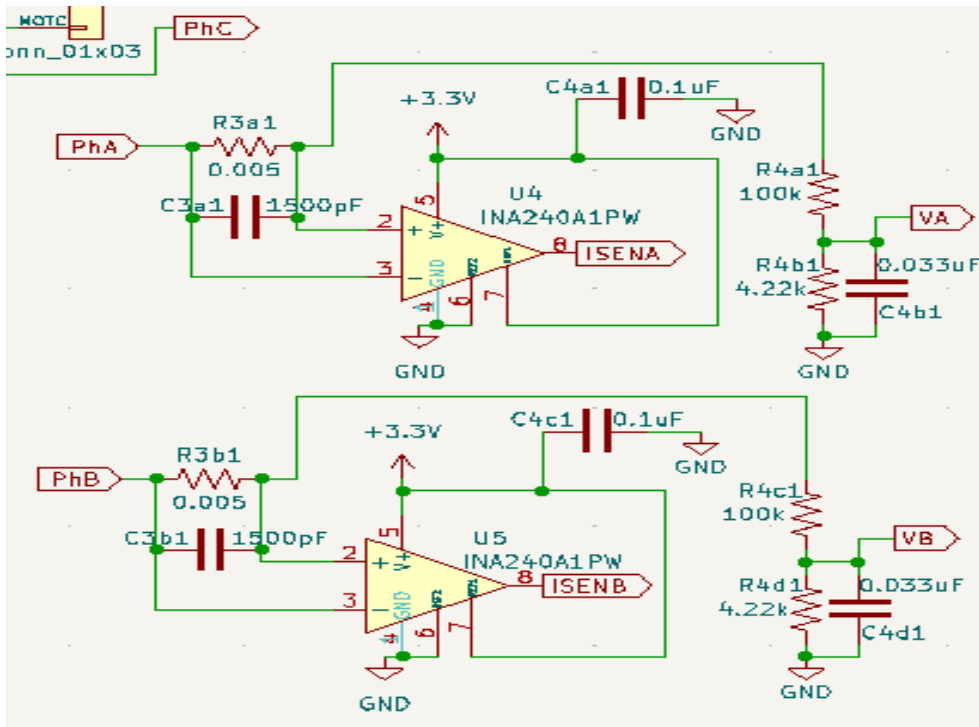


Figure 24 - Zoom on the phase voltage/current sense circuit.

Over Current Protection (OCP) circuit:

Three LM397 comparators is used to control the maximum value of the phase current of the motor. If one of the three currents exceeds, the output signal of the NOR port disables the related driver.

Low pass filter before comparators: $R=20\text{ohm}$ and $C=2200\text{pF}$ -> $\tau=44\text{ns}$.

Type of capacitors: Multilayer Ceramic Capacitor (MLCC), SMD/SMT, 25V, 0603, 1%.

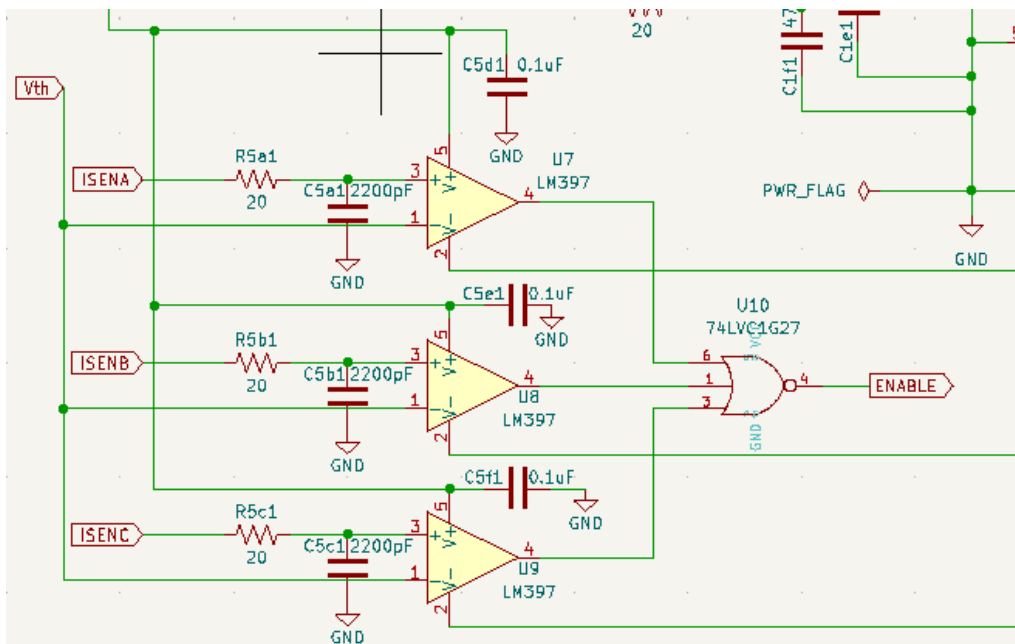


Figure 25 - Zoom on the Over Current Protection (OCP) circuit.

The NOR port used is the 74LVC1G27 [20], a single 3-input NOR gate. It is important to check the propagation delay in the datasheet of this device.

Table 15 - Dynamic characteristics table from the NOR port datasheet.

Symbol	Parameter	Conditions	-40°C to +85°C			-40°C to +125°C		Unit
			Min	Typ	Max	Min	Max	
t_{pd}	Propagation delay	VCC = 1.65 V to 1.95 V	1.5	4.7	20.5	1.5	25.7	ns
		VCC = 2.3 V to 2.7 V	1.0	3.0	7.1	1.0	8.9	ns
		VCC = 2.7 V	1.0	3.0	6.7	1.0	8.4	ns
		VCC = 3.0 V to 3.6 V	1.0	2.6	5.4	1.0	6.8	ns
		VCC = 4.5 V to 5.5 V	1.0	1.9	1.9	1.0	4.5	ns

In the dedicated section of the datasheet, there is a table where all the delay values are reported, measured in different V_{CC} ranges, and the worst case is 25.7ns. This value is however very small compared to the total switching period, which is 50000 ns.

Let consider that the total delay for one period is 236 ns (already discussed in the previous chapters, total delay = gate driver propagation delay + power MOSFET rise/fall). Adding the NOR delay to the total propagation delay, the result are still below 300 ns. So, the propagation delay of this logical port is acceptable and doesn't influence the overall system behaviour. The component is a good choice for this application.

POWER SUPPLIES: 3.3 – 5 – 48 V

Three levels of power are needed in the circuit.

The first is the 3.3 V supply used for all the logical part of the circuit.

The second is the 5 V reference which supplies the three gate drivers.

The last one is the 48 V, that is the nominal voltage of the motor and it is the supply of the power switches. So, the power MOSFETs are connected to the 48 V power supply, through a two-pin connector (one is the 48 V and second is the ground).

Instead, two DC/DC converters are used to obtain the other two power supplies.

The 3.3 V reference is obtained using the TPS54060 [17] buck converter (DC-DC step-down converter), which takes as input the 48 V power supply and gives as output the 3.3 V supply. The device, the passive components used for the application and the related connections are shown in the following schematic, which has been built in the schematic editor in KiCad (figure 24):

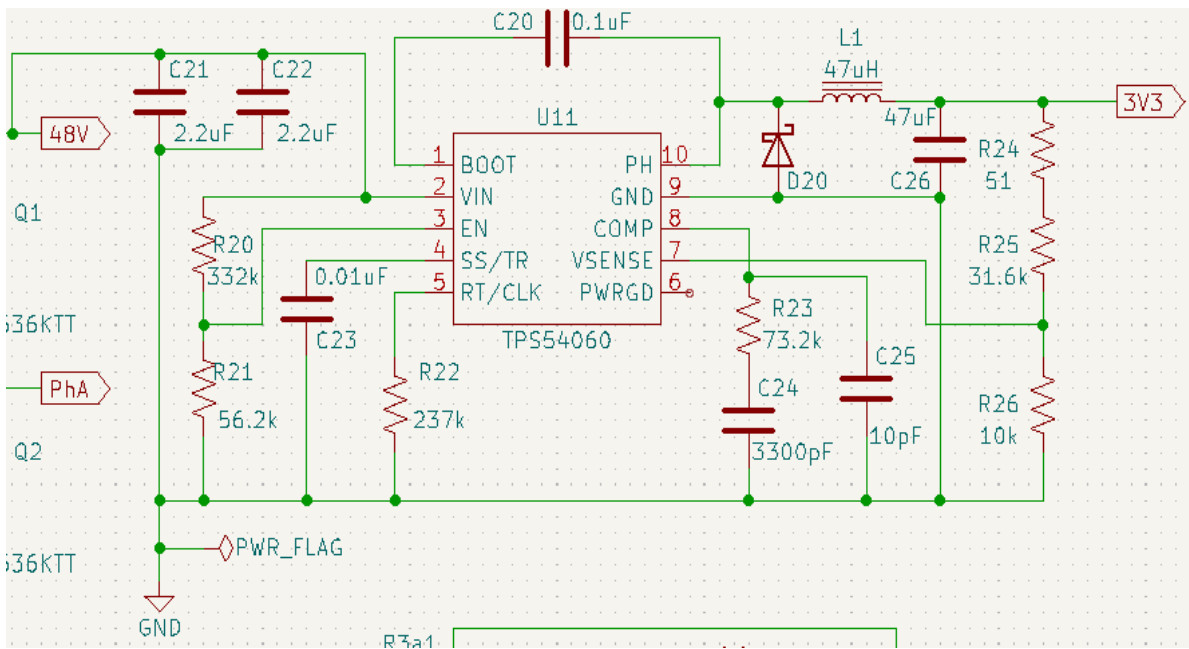


Figure 26 - Zoom on the DC/DC converter.

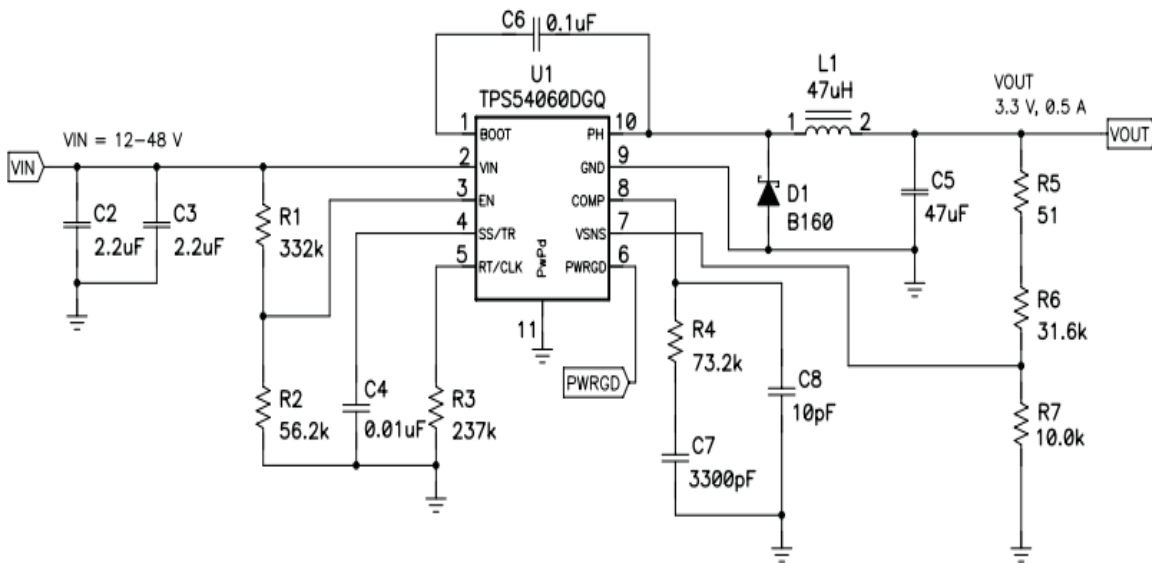


Figure 27 - DC-DC converter scheme from TPS54060 datasheet.

Some calculations dimensioning resistors and capacitors.

An important parameter is the switching frequency of the converter. In the datasheet there is a typical application and for this input and output voltage values an acceptable switching frequency can be about 500 kHz. The switching frequency is set by resistor R3, which is connected to the RT/CLK pin. To find the resistor value, the formula or the curve in the datasheet can be used:

$$R3 = \frac{206033}{(500kHz)^{1.0888}} = 237 \text{ k}\Omega$$

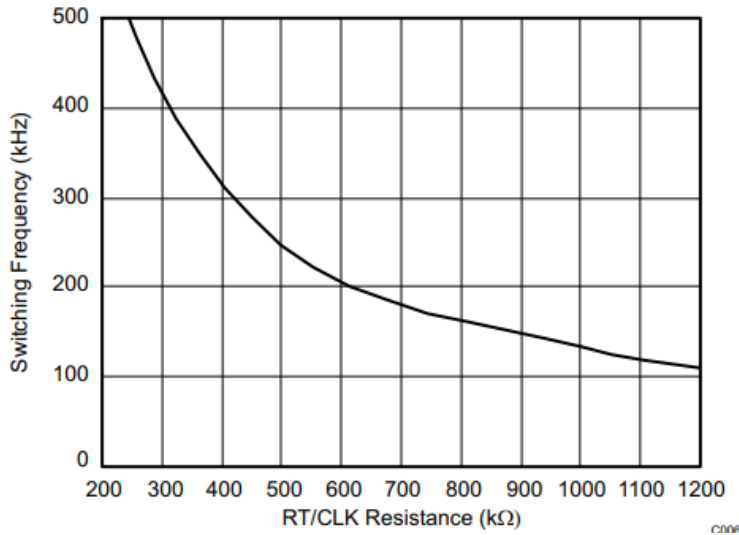


Figure 28 - f_{sw} vs RT/CLK resistance in low frequency range, from TPS54060 datasheet.

Bootstrap capacitor must be connected between the BOOT and PH pins for proper operation, $C_6 = 0.1 \mu\text{F}$. It is recommended to use a ceramic capacitor with X5R or better grade dielectric. The capacitor should have a 10 V or higher voltage rating.

The TPS54060 requires a high-quality ceramic, type X5R or X7R, input decoupling capacitor of at least $3 \mu\text{F}$, with at least a 60 V voltage rating is required to support the maximum input voltage. In this case two $2.2 \mu\text{F}$, 100 V capacitors in parallel have been selected (C_2 and C_3 , so the total capacitance is $4.4 \mu\text{F}$).

Adjusting the output voltage, starting from $R_7 = 10 \text{ k}\Omega$ and R_6 is calculated in this way:

$$R_6 = R_7 \times \frac{V_{out} - 0.8 \text{ V}}{0.8 \text{ V}} = 31.6 \text{ k}\Omega$$

Output inductor:

$$L_{o_{min}} = \frac{V_{in_{max}} - V_{out}}{I_o \times K_{ind}} \times \frac{V_{out}}{V_{in_{max}} \times f_{sw}}$$

for this design $K_{ind} = 0.3$ and the minimum inductor value is $39.7 \mu\text{H}$. A nearest standard value is chosen, $L_1 = 47 \mu\text{H}$. The MSS1048-473ML ($47 \pm 20\% \mu\text{H}$) shielded power inductor has been chosen, SMD component, $10.4 \times 10.4 \text{ mm}$ footprint (4.8 mm high).

Output capacitor (C_5): the most stringent criteria for the output capacitor is $15.2 \mu\text{F}$ of capacitance to keep the output voltage in regulation during a load transient. Additional capacitance de-ratings for aging, temperature and DC bias should be factored in which will increase this minimum value. A $47 \mu\text{F}$, 10 V, X5R ceramic capacitor will be used (with ESR = $5 \text{ m}\Omega$ and RMS ripple current = 37.7 mA).

Diode $D_1 = \text{B160A}$ Schottky (lower forward voltage, typical 0.50 V). It comes in a larger package size which has good thermal characteristics over small devices.

The slow start capacitor (C_4) of $0.01 \mu\text{F}$, connected to the SS/TR pin.

The programmable UVLO and enable voltages are set using a resistor divider between Vin and ground to the EN pin. To produce the 8.9 and 7.9 volt start and stop voltages, using datasheet equations, R1 = 332 kΩ (between Vin and EN) and R2=56.2 kΩ (between EN and GND).

For the compensation: crossover frequency (f_{co}) is 12.3 kHz. Three compensation components are added: a resistor in series with a capacitor is used to create compensating zero ($R_4 = 73.2 \text{ k}\Omega + C_7 = 3300 \text{ pF}$), a capacitor in parallel to these two components forms the compensating pole ($C_8 = 10 \text{ pF}$).

Then, 5 V power supply is needed for the gate drivers. In this case no additional converter is needed because in the Launchpad is already available a step-up voltage regulator (the LMR62421 device, the configuration is shown in the figure below). So, once the Launchpad is powered with 3.3 V supply, the 5 V reference is available in a specific connector pin.

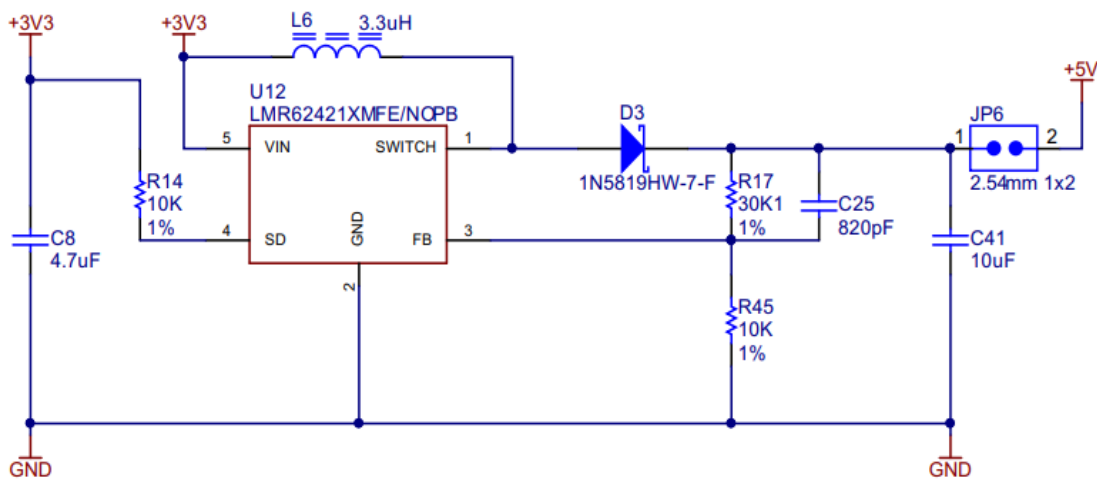


Figure 29 - Electrical circuit of the internal step-up voltage regulator (LMR62421) in the Launchpad.

FOOTPRINTS:

For each component of the electrical scheme, the most appropriate footprint has been assigned in KiCad. Then, all the footprints must be placed and linked together using tracks, to design the final PCB of the inverter.

CONNECTORS:

Launchpad connectors:

Two connectors Pin Socket 2x10, type: THT (through-hole technology), pitch = 2.54 mm.

Supply connector (two pins: 48 V and GND):

the same connector used for the motor, but instead of three pins only two pins are needed.

Motor connector (three pins: phase A, B and C):

The motor is connected to the PCB using T block.

Solution 1 -> PCB terminal block – PT 2,5 / 3 – 7,5 – V – 1987960

Some important characteristics from the datasheet:

nominal current = 32 A, nominal voltage = 800 V, nominal cross section = 2.5 mm², screw connection with wire protector, wave soldering, **pitch = 7.5 mm**, component dim = 13.5 × 22.5 × 13.1 mm, pin dim = 1 mm, hole diameter = 1.3 mm.

Solution 2 -> PCB terminal block – MKDSP 25 / 3 – 15,00 – 1932591

From datasheet:

nominal current = 125 A, nominal voltage = 1000 V, nominal cross section = 35 mm², screw connection with wire protector, wave soldering, **pitch = 15 mm**, component dim = 31 × 45 × 43.5 mm, pin dim = 1.2 mm, hole diameter = 1.6 mm, 4 solder pins per potential.

The second solution has been preferred because the connectors are more robust in terms of maximum currents and problems or damages can be avoided.

For all the other components I have chosen the **SMD** (surface-mounted device) type:

- DRIVERS: **UCC27282-Q1** ---> Package SON: Texas_DRC0010J_ThermalVias (10 pins)
- MOSFETS: **CSD19536KTT** ---> Package TO_SOT: TO-263-3_TabPin4 (4 pins)
- COMPARATOR: **LM397** ---> Package TO_SOT: SOT-23-5 (5 pins)
- AMPLIFIER: **INA240A1PW** ---> Package SO: TSSOP-8 (4.4x3mm_PO.65mm) (8 pins)
- NOR PORT: **74LVC1G27** ---> Package TO_SOT: SOT-886 (6 pins)
- DC-DC CONVERTER: **TPS54060** ---> Package SO: HVSSOP (3x3mm_PO.5mm) (10 pins)
- CAPACITORS: C_0805_2012Metric_Pad1.18x1.45mm_HandSolder
(For 2.2uF capacitors: C_1210_3225Metric_Pad1.33x2.70mm_HandSolder)
- RESISTORS: R_0805_2012Metric_Pad1.20x1.40mm_HandSolder
- DIODES: D_0805_2012Metric_Pad1.15x1.40mm_HandSolder

Board Settings ---> Board Layer Stackup

The board is composed of **four layers (F.Cu, B.Cu, In1.Cu and In2.Cu)**.

In the board settings some parameters related to the layers characteristics can be modified. For example, the thickness is set for each layer:

F.Cu (Front Copper Layer) = 0.07 mm; In1.Cu (first internal copper layer) = 0.07 mm;

In2.Cu (second internal copper layer) = 0.07 mm; B.Cu (Back Copper Layer) = 0.07 mm.

Copper layers: 4 Impedance controlled

Layer	Id	Type	Material	Thickness
■	F.Silkscreen	Top Silk Screen	Not specified	
■	F.Paste	Top Solder Paste		
■	F.Mask	Top Solder Mask	Not specified	0.01 mm
■	F.Cu	Copper		0.07 mm
■	Dielectric 1	Core	FR4	1.51 mm
■	In1.Cu	Copper		0.07 mm
■	Dielectric 2	Core	FR4	1.51 mm
■	In2.Cu	Copper		0.07 mm
■	Dielectric 3	Core	FR4	1.51 mm
■	B.Cu	Copper		0.07 mm
■	B.Mask	Bottom Solder Mask	Not specified	0.01 mm
■	B.Paste	Bottom Solder Paste		
■	B.Silkscreen	Bottom Silk Screen	Not specified	

Board thickness from stackup: 4.83 mm

Figure 30 - Board stackup – Physical stackup from PCB editor.

The total board thickness is **4.83 mm**, considering the three **dielectric layers** (1.51 mm) that act as **insulators** between the copper layers (also adding 0.01 mm of F.Mask and B.Mask, top and bottom solder masks).

Components location:

Some important considerations placing the components in the PCB.

The hot devices, which are the 6 power MOSFETs, must be placed away from precision devices, which are the three sensing resistors and the NOR port.

Another important stuff is that the low pass filters and in general all the capacitors in the PCB must be placed so close to their sink, to avoid filter problems or instability of the important logical signals.

Finally, it is a right rule to place the supply voltage and the motor connectors quite far with respect to the Launchpad because the power sources could cause some problems if they are so close to the controller zone, where the power is much lower.

The Launchpad size is 130x59mm, and it is placed in the left-bottom corner of the PCB and it is shown in the bottom figure where there are the two connectors that are placed according to the distances described in the microcontroller datasheet.

The location of the motor and the power supply connectors can be also verified. The motor connector is in the right part of the PCB because it is close to the power MOSFETs. The power supply connector is in the top part but both the connectors, as previously said, are quite far from the Launchpad connectors.

The overall size of the PCB is 260x150mm.

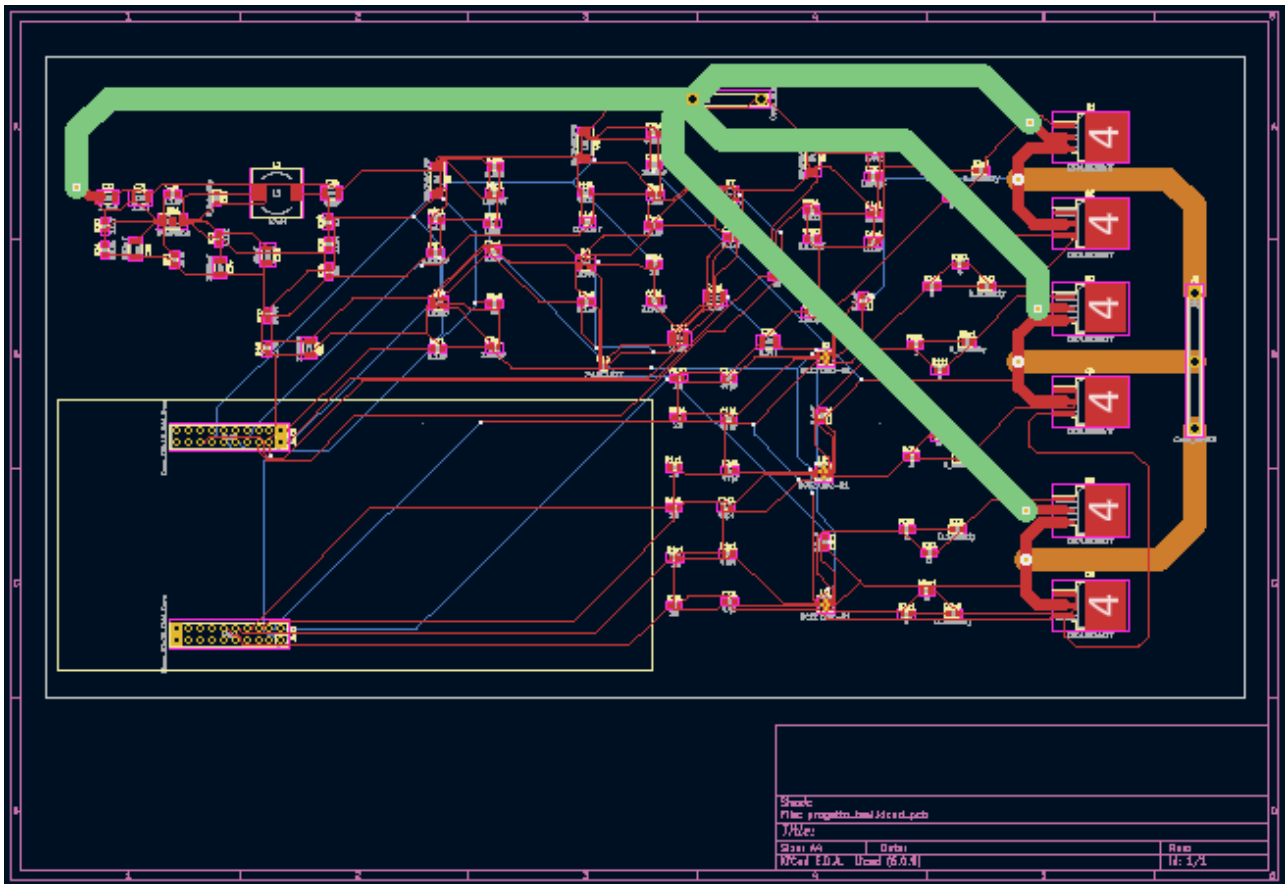


Figure 31 - Printed Circuit Board of the total inverter with all the footprints and the tracks, screen taken from PCB editor in KiCad.

TRACKS:

The track width is **0.25 mm** for all the tracks used for the signals, these tracks are all in the main layers which are the front copper layer (in the figure 17 are the red tracks) and the back copper layer that is the ground planes (in the figure 17 are the blue tracks).

Instead for the power tracks which connect the motor connectors to the MOSFET outputs and also for the connection between the power supply and the power devices the width should be increased up to **10 mm** but this is a big problem because there would be no space to trace them.

This is why the layer thickness is doubled, from 35 micron to 70 micron, and there are four copper layers instead to have a simple two layers PCB. In fact, increasing the layer thickness implies a reduction in width value.

Since the tracks are still wide the other two additional layers can be used for the power tracks.

The two further power copper planes can be added in order to dissipate the heat generated by power tracks.

At the end, the final width of the power tracks is **5 mm** and they are drawn on the two internal layers. One practical way to connect the MOSFET pin to the motor connector is through a layer change.

In particular, the solution involves tracing a short track from the MOSFET pin, which connects to a via to pass to the underlying layer (the orange one in the figure), where a much wider track is traced that reaches the motor connector. The short track is 2.5 mm wide and the via has the diameter of 2.5 mm and the hole of 0.8 mm.

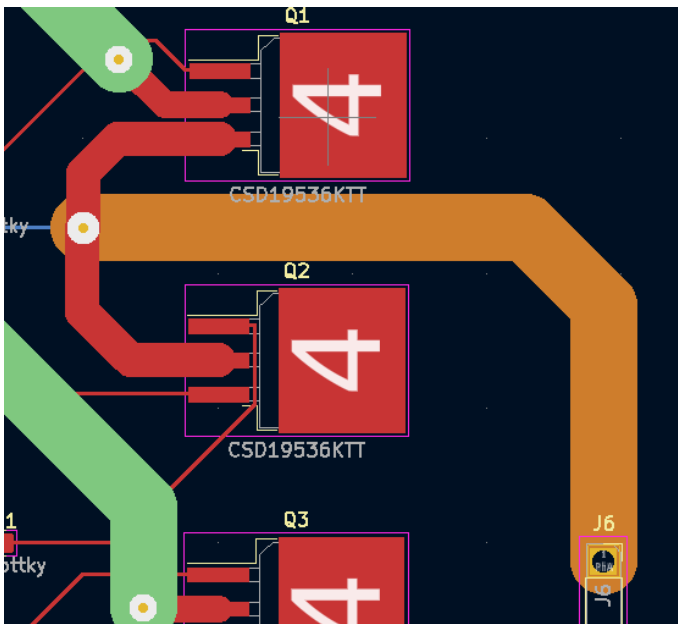


Figure 32 - zoom on the motor power tracks.

The advantage of using a layer switch to connect the MOSFET to the motor is that it allows enough space for the track, which must be of adequate width to handle the current required to operate the motor.

Also, choosing a short path from the MOSFET pin to the via reduces electromagnetic noise and improves the quality of the transmitted signal, helping to improve circuit reliability.

The same procedure has been done for the power supply tracks. In this case the internal layer used for the power tracks is the In1.Cu which is the green one shown in the figure.



Figure 33 - zoom on the supply power tracks.

All the other via used in the PCB to change from the F.Cu layer to the B.Cu ground layer are smaller (respect to the ones used for the power tracks) and they have a diameter of 0.8 mm and a hole of 0.4 mm.

MOSFET heatsink:

The last important consideration is about the MOSFET overheating, it is important to check in the CSD19536KTT datasheet the thermal information.

The two main parameters are the thermal resistances (junction-to-case and junction-to-ambient).

$R_{\theta JC}$, Junction-to-case thermal resistance = 0.4 °C/W

$R_{\theta JA}$, Junction-to-ambient thermal resistance = 62 °C/W

Then, it needs to calculate the total dissipated power by the MOSFET which can be calculated as follow:

$$P = I^2 \times R_{DS(on)} = (80A)^2 \times 2m\Omega = 12.8W$$

$$\text{Maximum junction temperature: } T_j = T_a + (P \times R_{\theta JA}) = 25^\circ C + (12.8W \times 62^\circ C/W) = 818.6^\circ C$$

This temperature is much higher than the maximum temperature permitted by the power device, which is 175°C (specified in the datasheet).

A heat sink for each power MOSFET should be added to dissipate this large amount of heat.

A heat sink with a sufficient low thermal resistance must be selected in order to dissipate the total power generated by the MOSFET and keep the temperature below the maximum permitted limit.

The thermal impedance of the heat sink can be chosen using this equation:

$\Delta T_{max} = T_{jmax} - T_a = 175^\circ C - 50^\circ C = 125^\circ C$, where ΔT_{max} is the maximum temperature increase that is the difference between the maximum junction temperature and the maximum ambient temperature.

$R_{\theta JA} = 125^{\circ}\text{C} / 12.8\text{W} = 9.76^{\circ}\text{C}/\text{W}$, so this can be a plausible value for the thermal impedance of the heat sink.

The heat sink chosen for this type of MOSFET is the 26176CTE component.

This heat sink is designed for the D2PAK TO-263, which is the MOSFET package.

Also, the dimensions of the heat sink must be considered if they should be put in the correct way.

All the important parameters are shown in the device datasheet and in the bottom table.

Table 16 - Heat sink parameters from the datasheet.

26176CTE Heat sink specifications	
Material	Copper
Finish	Matte Tin
Device Cooled	TO-263
Thermal resistance	11.00 °C/W
Length	19.38 mm
Width	25.40 mm
Height	11.43 mm

This is the last component which has been added to the PCB to avoid the MOSFET overheating.

The design process is finished, so the PCB is complete.

3.2. Bill of materials

The following table lists the PCB bill of materials (BOM).

This is very useful to check the main characteristics of each device used in the printed circuit board. For each component the part number, the quantity, the reference designator, the manufacturer, a short description, the package type and size.

In the last two columns there are the link where the component can be bought and the estimated cost of the device.

Table 17 - Inverter PCB bill of materials

ITEM #	QTY	REF DES	MANUFACTURER	MAN PART NUM	DESCRIPTION	PACKAGE	TYPE	PURCHASE LINK	ESTIMATED COST
1	1	PCB			Inverter PCB: 4 layers, 260x150mm				
2	3	U1, U2, U3	Texas Instruments	UCC27282-Q1	Half-Bridge Driver, 3A 120V	SON, Texas DRC0010J with thermal vias	SMT	https://www.mouser.it/ProductDetail/Texas-Instruments/UCC27282QDQ1?qs=bAKSY%2FctAC5mavLE05ocrw%3D%3D	1.95 €
3	6	Q1, Q2, Q3, Q4, Q5, Q6	Texas Instruments	CSD19536KTT	N-Channel NexFET 100V Power MOSFET	D2PAK, TO-263, TabPin4	SMT	https://www.mouser.it/ProductDetail/Texas-Instruments/CSD19536KTT?qs=MiqG6Kq1qKP2NIsb3jZrDg%3D%3D	4.76 €
4	2	J1J3, J4J2	Samtec	HLE-107-02-G DV-BE-LC-K-TR	Connector, Pin Socket, Straight, Female, 2x10 Pin, 2.54mm pitch			https://www.mouser.it/ProductDetail/Samtec/HLE-107-02-G-DV-BE-LC-K-TR?qs=3%252BjIH0OdpA9jJzYaMd%252BC9A%3D%3D	3.30 €
5	1	J5	Phoenix Contact	MKDSP 25/ 2-15,00 - 1932588	Connector, Pin Socket, Straight, Female, 1x2 Pin, 2.54mm pitch			https://www.mouser.it/ProductDetail/Phoenix-Contact/1932588?qs=zGjMOL9s0Z%252BnZxcpLOCAEA%3D%3D	13.28 €
6	1	J6	Phoenix Contact	MKDSP 25/ 3-15,00 - 1932591	Connector, Pin Socket, Straight, Female, 1x3 Pin, 2.54mm pitch			https://www.mouser.it/ProductDetail/Phoenix-Contact/1932591?qs=XyR8odSBc%252Bd8y8FLAurifg%3D%3D	19.33 €
7	1	U11	Texas Instruments	TPS54060DGQ	Step-Down DC-DC Converter, 0.5A 60V	HVSSOP, 10 pins, 3x3mm, 0.5mm pitch	SMT	https://www.mouser.it/ProductDetail/Texas-Instruments/TPS54060DGQ	2.81 €

								Instruments/TPS54060DGQ?qs=3bSaU8eFeoEBCFD0I39Oew%3D%3D	
8	3	U4, U5, U6	Texas Instruments	INA240A1PW	Bidirectional, Ultra-Precise Current Sense Amplifier (-4V to 80V)	TSSOP, 8 pins, 4.4x3mm, 0.65mm pitch	SMT	https://www.mouser.it/ProductDetail/Texas-Instruments/INA240A1PW?qs=aVvJF2WnoUQ4CUqAxLDbhw%3D%3D	3.83 €
9	3	U7, U8, U9	Texas Instruments	LM397MF	Single General-Purpose Voltage Comparator	SOT-23, 5 pins, 2.9x1.6mm	SMT	https://www.mouser.it/ProductDetail/Texas-Instruments/LM397MF?qs=QbsRYf82W3HWtoAsLY4Yxg%3D%3D	1.68 €
10	1	U10	Nexperia	74LVC1G27GM, 115	Single 3 input NOR gate	SOT-886, XSON6	SMT	https://www.mouser.it/ProductDetail/Nexperia/74LVC1G27GM115?qs=NQoTdinTi9FEdnCzEG9pQA%3D%3D	0.37 €
11	6	R1a, R1b, R1c, R1d, R1e, R1f	ROHM Semiconductor	SFR10EZPF2OR0	Thick film resistor	RES, 20R, ±1%, 1/8 W, SMD0805	SMT	https://www.mouser.it/ProductDetail/ROHM-Semiconductor/SFR10EZPF2OR0?qs=amGC7iS6iy9v9oiskVWmDg%3D%3D	0.18 €
12	6	C1a, C1b, C1c, C1d, C1e, C1f	Vishay/Vitramon	VJ0805A470JXXCW1BC	Multilayer ceramic capacitor	CAP, 47PF, ±5%, 25V, COG, SMD0805	SMT	https://www.mouser.it/ProductDetail/Vishay-Vitramon/VJ0805A470JXXCW1BC?qs=idbaOeilTkP5DL8zhWE88A%3D%3D	0.16 €
13	3	C1g, C1h, C1i	KEMET	C1210C225J3RACTU	Multilayer ceramic capacitor	CAP, 2.2UF, ±5%, 25V, X7R, SMD1210	SMT	https://www.mouser.it/ProductDetail/KEMET/C1210C225J3RACTU?qs=z33Fpd7anBCDbKlrlXf%2FrA%3D%3D	1.40 €
14	6	R2a, R2b, R2c, R2d, R2e, R2f, R2g, R2h, R2i, R2j, R2m, R2n	Royalohm	0805W8F500KT5E	Thick film resistor	RES, 5R, ±1%, 1/8 W, SMD0805	SMT	https://www.mouser.it/ProductDetail/Royalohm/0805W8F500KT5E?qs=e8oIoAS2J1SPOQGhQuicLA%3D%3D	0.18 €
15	3	C2a, C2b, C2c	Murata Electronics	GCM21BR71E104JA37L	Multilayer ceramic capacitor	CAP, 0.1UF, ±5%, 25V, X7R, SMD0805	SMT	https://www.mouser.it/ProductDetail/Murata-Electronics/GCM21BR71E104JA37L?qs=ui%252B2d9IVEI7OYh7A7OY47Q%3D%3D	0.35 €
16	6	D2a, D2d, D2e, D2h, D2i, D2n	KYOCERA AVX	SD0805S040S0R1	Schottky Diode	DIODE, 40V, 0.1A, SMD0805, -65/+125°C (forward voltage = 0.5V)	SMT	https://www.mouser.it/ProductDetail/KYOCERA-AVX/SD0805S040S0R1?qs=jCA%252BPfw4LHYgtNhiwPuw4Q%3D%3D	0.45 €
17	1	L1	Coilcraft	MSS1048-473MLC	Inductor	Power Inductor, shielded, 47UH, 2.2A, 0.12Ω, 10X10X4.8mm, SMD	SMT	https://www.mouser.it/ProductDetail/Coilcraft/MSS1048-473MLC?qs=zCSbvcPd3pYD3eDAqEg4Jg%3D%3D	2.39 €

18	1	D20	Diodes Incorporated	B160AE-13	Schottky Diode	DIODE, 60V, 1A, DO-214AA, -55/+150°C (forward voltage = 0.65V)	SMT	https://www.mouser.it/ProductDetail/Diodes-Incorporated/B160AE-13?qs=AQIKX63v8Rtd1YKJNyOSAO%3D%3D	0.32 €
19	2	C21, C22	KEMET	C1210X225J1RACTU	Multilayer ceramic capacitor	CAP, 2.2UF, ±5%, 100V, X7R, SMD1210	SMT	https://www.mouser.it/ProductDetail/KEMET/C1210X225J1RACTU?qs=s6nfgz3miVxtipcuBgp61w%3D%3D	0.86 €
20	1	C20	TAIYO YUDEN	UMK212BJ104KGHT	Multilayer ceramic capacitor	CAP, 0.1UF, ±10%, 50V, X5R, SMD0805	SMT	https://www.mouser.it/ProductDetail/TAIYO-YUDEN/UMK212BJ104KGHT?qs=CNQs48zzdnrlin01Ff2Q8Q%3D%3D	0.11 €
21	1	C26	KYOCERA AVX	1210ZD476KAT2A	Multilayer ceramic capacitor	CAP, 47UF, ±10%, 10V, X5R, SMD1210	SMT	https://www.mouser.it/ProductDetail/KYOCERA-AVX/1210ZD476KAT2A?qs=XLNwXgtzMM%252BFPb3B3eYuZA%3D%3D	1.04 €
22	1	C23	KYOCERA AVX	1210ZC103KAT9ZM	Multilayer ceramic capacitor	CAP, 0.01UF, ±10%, 10V, X7R, SMD1210	SMT	https://www.mouser.it/ProductDetail/KYOCERA-AVX/1210ZC103KAT9ZM?qs=N6dQCmPuaqkPJ2o2WvYepw%3D%3D	0.07 €
23	1	C24	KYOCERA AVX	1210YC332KAT2A	Multilayer ceramic capacitor	CAP, 3.3NF, ±10%, 16V, X7R, SMD1210	SMT	https://www.mouser.it/ProductDetail/KYOCERA-AVX/1210YC332KAT2A?qs=ljDp%252B3tRSNOb3X7RrHR%252BQA%3D%3D	0.33 €
24	1	C25	KEMET	C1210C100J8HACAUTO	Multilayer ceramic capacitor	CAP, 10PF, ±5%, 10V, X8R, SMD1210	SMT	https://www.mouser.it/ProductDetail/KEMET/C1210C100J8HACAUTO?qs=i%252B1pi9TdxUZrkaVKhWyieg%3D%3D	0.29 €
25	1	R20	Bourns	CR0805-FX-3323ELF	Thick film resistor	RES, 332K, ±1%, 1/8 W, SMD0805	SMT	https://www.mouser.it/ProductDetail/Bourns/CR0805-FX-3323ELF?qs=4vGxhLEmbUyIm%2FJsSp83gA%3D%3D	0.09 €
26	1	R21	Vishay/Dale	CRCW080556K2FKEAC	Thick film resistor	RES, 56.2K, ±1%, 1/8 W, SMD0805	SMT	https://www.mouser.it/ProductDetail/Vishay-Dale/CRCW080556K2FKEAC?qs=E3Y5ESvWgWNWd9iOC9Wsag%3D%3D	0.15 €
27	1	R22	Bourns	CR0805-FX-2373ELF	Thick film resistor	RES, 237K, ±1%, 1/8 W, SMD0805	SMT	https://www.mouser.it/ProductDetail/Bourns/CR0805-FX-2373ELF?qs=Woncl1%2FfcWdj%2FiUaDp8LAMw%3D%3D	0.09 €
28	1	R23	Bourns	CR0805-FX-7322ELF	Thick film resistor	RES, 73.2K, ±1%, 1/8 W, SMD0805	SMT	https://www.mouser.it/ProductDetail/Bourns/CR0805-FX-7322ELF?qs=Ek4EPvi0xiAE7rWvr1NJyw%3D%3D	0.09 €

29	1	R24	Bourns	CR0805-FX-51R0ELF	Thick film resistor	RES, 51R, ±1%, 1/8 W, SMD0805	SMT	https://www.mouser.it/ProductDetail/Bourns/CR0805-FX-51R0ELF?qs=LA9FZBosJlDgljB9k%2FNAMg%3D%3D	0.09 €
30	1	R25	Bourns	CR0805-FX-3162ELF	Thick film resistor	RES, 31.6K, ±1%, 1/8 W, SMD0805	SMT	https://www.mouser.it/ProductDetail/Bourns/CR0805-FX-3162ELF?qs=4vGXhLEmbUxw0LplaWR6Eg%3D%3D	0.09 €
31	1	R26	Bourns	CR0805-FX-1002ELF	Thick film resistor	RES, 10K, ±1%, 1/8 W, SMD0805	SMT	https://www.mouser.it/ProductDetail/Bourns/CR0805-FX-1002ELF?qs=tknLyCMIRbPr%252BDD0s0nG9g%3D%3D	0.09 €
32	3	R3a, R3b, R3c	YAGEO	AA0805FR-075M1L	Thick film resistor	Sensing resistor, 5.1mOhm, ±1%, 1/8 W, SMD0805, 150 PPM/°C	SMT	https://www.mouser.it/ProductDetail/YAGEO/AA0805FR-075M1L?qs=9h0bZHM%2F3zIYgJpwPaiHEw%3D%3D	0.10 €

This table is very useful because shows all the components used to build the final PCB.

The designer can use this table to buy all the components needed by clicking on the link in the second-last column.

All the links lead to the Mouser website where each single or more than one type of component can be purchased.

In the last column there is the price of each single component. This price must be multiplied by the quantity and then, if all prices are added together the total estimated cost can be derived to have an idea of the total cost of the PCB. Obviously, the production cost of the printed circuit board must be added to the total cost.

4. Conclusions

This project thesis has been done to have an inverter which control a 48V electric motor with high currents, more than 80A peak currents.

It has been demonstrated that the designed inverter is able to manage these currents and in general the involved powers. In fact, in the simulation section, the worst case of high current situation has been tested and the graphs show that the sink and source currents which the gate drivers must exchange are within the limits of the component. The gate driver selected is the UCC27282-Q1 and the peak source and sink output currents are up to 3A. From the Simulink simulation can be verified that the maximum current flowing between the gate driver and power MOSFETs is 1A. This value is very far from the maximum accepted by the driver this device is definitely capable to drive the power switches.

The same can be said for the power MOSFETs used which are very resistant for this application. These power devices are able to handle the motor currents and they have very low switching losses.

The final check is about the total delay during the switching period. It is important to verify that this parameters is not very big respect to the total period. All the component delays are reported and summed in a delay table to demonstrate that the total delay of the system doesn't cause unexpected behaviours. With the final configuration this value is less then 300ns and this is a good result because the switching period is 50 μ s (1/20 kHz). The total delay is 0.6% of the switching period and this doesn't affect the normal operating condition.

It can therefore be concluded that the system works correctly and safely, the motor is supplied and controlled as expected.

Before producing the PCB, it would be good practice to do a thermal validation that verifies that all the components and in general the PCB does not overheat, this phase must be executed to avoid damage in the board during testing.

At the end the PCB can be really produced and connected to the electric motor for testing and checking that the overall system works properly also in real applications.

5. References

1. Hasan, Mubashwar, Saad Mekhilef, and Mahrous Ahmed. "Three-phase hybrid multilevel inverter with less power electronic components using space vector modulation." *IET Power Electronics* 7.5 (2014): 1256-1265.
2. Y. Chen, J. Du, L. Feng, J. Xiao, J. Zhang and Y. He, "Comparative Study on Driving Switching Characteristics of GaN-FET and SiC-MOSFET in Transient High Voltage Pulse Discharge Circuit," 2020 IEEE International Conference on High Voltage Engineering and Application (ICHVE), Beijing, China, 2020, pp. 1-4, doi: 10.1109/ICHVE49031.2020.9279479.
3. Rabkowski, Jacek, Dimosthenis Pefitsis, and Hans-Peter Nee. "Silicon carbide power transistors: A new era in power electronics is initiated." *IEEE Industrial Electronics Magazine* 6.2 (2012): 17-26.
4. R. Pradhan, N. Keshmiri and A. Emadi, "On-Board Chargers for High-Voltage Electric Vehicle Powertrains: Future Trends and Challenges," in *IEEE Open Journal of Power Electronics*, vol. 4, pp. 189-207, 2023, doi: 10.1109/OJPEL.2023.3251992.
5. Beheshti, Masoud. "Wide-bandgap semiconductors: Performance and benefits of GaN versus SiC." *Analog Des. J* 4 (2020): 1-6.
6. Texas Instruments, "DRV832x 6 to 60-V Three-Phase Smart Gate Driver" DRV8323 datasheet, Feb. 2017 [Revised March 2002].
7. Cole Macias, "System Design Considerations for High-Power Motor Driver Applications" Texas Instruments Application Report, June 2021.
8. Nicholas Oborny, Ashish Ojha, "Understanding Smart Gate Drive" Texas Instruments Application Report, June 2015 [Revised March 2021].
9. Mateo Begue, High Power Drivers, "External Gate Resistor Design Guide for Gate Drivers" Texas Instruments Technical Notes, May 2018 [Revised March 2020].
10. Laszlo Balogh, "Fundamentals of MOSFET and IGBT Gate Driver Circuits" Texas Instruments Application Report, March 2017 [Revised Oct. 2018].
11. Texas Instruments, "LAUNCHXL-F28379D Overview" User's Guide, Aug. 2016 [Revised March 2019].
12. Texas Instruments, "UCC27282-Q1 Automotive 3-A 120-V Half-Bridge Driver with Cross Conduction Protection and Low Switching Losses" UCC27282-Q1 datasheet, Sept. 2019 [Revised Oct. 2002].
13. Texas Instruments, "CSD88599Q5DC 60-V Half-Bridge NexFET™ Power Block" CSD88599Q5DC datasheet, April 2017 [Revised April 2018].
14. Texas Instruments, "CSD19536KTT 100-V N-Channel NexFET™ Power MOSFET" CSD19536KTT datasheet, March 2015 [Revised Aug. 2016].
15. Texas Instruments, "CSD19535KCS 100 V N-Channel NexFET™ Power MOSFET" CSD19535KCS datasheet, Jan. 2014 [Revised Oct. 2014].
16. Texas Instruments, "CSD18536KCS 60 V N-Channel NexFET™ Power MOSFET" CSD18536KCS datasheet, March 2015 [Revised Dec. 2017].

17. Texas Instruments, "TPS54060 0.5-A, 60-V Step Down DC-DC Converter with Eco-Mode™" TPS54060 datasheet, Jan. 2009 [Revised Sept. 2015].
18. Texas Instruments, "LM397 Single General-Purpose Voltage Comparator" LM397 datasheet, May 2001 [Revised May 2016].
19. Texas Instruments, "INA240 –4-V to 80-V, Bidirectional, Ultra-Precise Current Sense Amplifier With Enhanced PWM Rejection" INA240 datasheet, July 2016 [Revised Dec. 2021].
20. NXP Semiconductors, "74LVC1G27 Single 3-input NOR gate" 74LVC1G27 datasheet, Feb. 2012.